How to Calculate Molecular Column Density

JEFFREY G. MANGUM

National Radio Astronomy Observatory, 520 Edgemont Road, Charlottesville, VA 22903;
jmangum@nrao.edu

YANCY L. SHIRLEY

Steward Observatory, University of Arizona, 933 North Cherry Avenue, Tucson, AZ 85721;
yshirley@as.arizona.edu

ABSTRACT. The calculation of the molecular column density from molecular spectral (rotational or ro-vibrational) transition measurements is one of the most basic quantities derived from molecular spectroscopy. Starting from first principles where we describe the basic physics behind the radiative and collisional excitation of molecules and the radiative transfer of their emission, we derive a general expression for the molecular column density. As the calculation of the molecular column density involves a knowledge of the molecular energy level degeneracies, rotational partition functions, dipole moment matrix elements, and line strengths, we include generalized derivations of these molecule-specific quantities. Given that approximations to the column density equation are often useful, we explore the optically thin, optically thick, and low-frequency limits to our derived general molecular column density relation. We also evaluate the limitations of the common assumption that the molecular excitation temperature is constant and address the distinction between beam-averaged and source-averaged column densities. As non-LTE approaches to the calculation of molecular spectral line column density have become quite common, we summarize non-LTE models that calculate molecular cloud volume densities, kinetic temperatures, and molecular column densities. We conclude our discussion of the molecular column density with worked examples for $C^{18}O$, $C^{17}O$, N_2H^+, NH_3, and H_2CO. Ancillary information on some subtleties involving line profile functions, conversion between integrated flux and brightness temperature, the calculation of the uncertainty associated with an integrated intensity measurement, the calculation of spectral line optical depth using hyperfine or isotopologue measurements, the calculation of the kinetic temperature from a symmetric molecule excitation temperature measurement, and relative hyperfine intensity calculations for NH_3 are presented in appendices. The intent of this document is to provide a reference for researchers studying astrophysical molecular spectroscopic measurements.

1. INTRODUCTION

Molecular spectral line column densities are fundamental to the study of the physical and chemical conditions within dense molecular clouds. Chemical composition, molecular isomer and isotopomer ratios, molecular hydrogen column densities, and molecular volume densities are all based on a measure of the molecular column density. Past reviews and tutorials on this subject, including Genzel (1991), Evans et al. (1991), Evans (1999), and Goldsmith & Langer (1999), along with spectroscopic textbooks such as Townes & Schawlow (1975), Gordy & Cook (1984), and Draine (2011) have provided an excellent basis upon which one can derive the molecular spectral line column density for a variety of dense molecular cloud environments. The intent of this tutorial is to provide students and scientists a general single reference point for the calculation of the molecular spectral line column density.

We have organized the document such that some basic background information is first provided to allow a contextural foundation to be lain for further calculations. This foundation includes a basic understanding of radiative transfer and statistical equilibrium (§§ 2 and 3), molecular degeneracy (§§ 5 and 6), partition functions (§ 7), line strength (§§ 8 and 9), and hyperfine structure (§ 10). The derivation of the most general form of the molecular spectral line column density is presented in § 4. We also explore a number of commonly used practical approximations to the calculation of the molecular spectral line column density in § 11. As the calculation of the molecular spectral line column density normally assumes constant excitation temperature, we address the consequences of this assumption when non-LTE conditions are present in § 12. We also summarize non-LTE approaches to the calculation of molecular cloud volume density, kinetic temperature, and molecular column density in § 13.

Molecular cloud structure and its relationship to the spatial resolution of a measurement system affects the derivation of molecular spectral line column density. To quantify these effects,

we address the distinction between beam-averaged and source-averaged column density in § 14.

As worked examples are often illustrative for many astrophysical calculations, in § 15 we provide step-by-step derivations of the molecular column density for several representative molecules, including $C^{18}O$, $C^{17}O$, N_2H^+, NH_3, and H_2CO. Appendices provide ancillary information on some subtleties often encountered when calculating molecular spectral line column density, including line profile functions (Appendix A), conversion between integrated flux and brightness temperature (Appendix B), the calculation of the uncertainty associated with an integrated intensity measurement (Appendix C), the calculation of spectral line optical depth using hyperfine or isotopologue measurements (Appendix D), the calculation of the kinetic temperature from a symmetric molecule excitation temperature measurement (Appendix E), and relative hyperfine intensity calculations for NH_3 (Appendix F).

2. RADIATIVE AND COLLISIONAL EXCITATION OF MOLECULES

When the energy levels of a molecule are in statistical equilibrium, the rate of transitions populating a given energy level is balanced by the rate of transitions which depopulate that energy level. For a molecule with multiple energy levels, statistical equilibrium can be written as:

$$n_i \sum_j R_{ij} = \sum_j n_j R_{ji}, \tag{1}$$

where n_i and n_j are the populations of the energy levels i and j and R_{ij} and R_{ji} are transition rates between levels i and j. The transition rates contain contributions from:

1. Spontaneous radiative excitation (A_{ij})
2. Stimulated radiative excitation and de-excitation [$R_{ij} \equiv n_i B_{ij} \int_0^\infty J_\nu \phi_{ij}(\nu) d\nu$]
3. Collisional excitation and de-excitation ($n_{\text{collider}} C_{ij}$)

where $\phi_\nu(\nu)$ is the line profile function and J_ν is defined as the integral of the specific intensity I_ν over the source of emission:

$$J_\nu \equiv \frac{1}{4\pi} \int I_\nu d\Omega. \tag{2}$$

Our statistical equilibrium equation then becomes:

$$n_i \left[\sum_j (n_{\text{collider}} C_{ij} + B_{ij} \int_0^\infty J_\nu \phi_{ij}(\nu) d\nu) + \sum_{j<i} A_{ij} \right]$$
$$= \sum_j n_j (n_{\text{collider}} C_{ij} + B_{ji} \int_0^\infty J_\nu \phi_{ji}(\nu) d\nu) + \sum_{j>i} n_j A_{ji}. \tag{3}$$

For a two-level system with i defined as the lower energy level l and j defined as the upper energy level u, $\sum_{j<i} A_{ij} = 0$ and the statistical equilibrium equation (eq. [3]) becomes:

$$n_l(n_{\text{collider}} C_{lu} + B_{lu} \int_0^\infty J_\nu \phi_{lu}(\nu) d\nu)$$
$$= n_u(n_{\text{collider}} C_{ul} + B_{ul} \int_0^\infty J_\nu \phi_{ul}(\nu) d\nu + A_{ul}). \tag{4}$$

As hydrogen (H) is the most abundant atom in the interstellar medium, and in dense molecular clouds most of the H is in molecular form (H_2), n_{collider} is usually assumed to be $n(H_2)$.

At this point, we can derive the Einstein relations A_{ul}, B_{ul}, and B_{lu} by considering only radiative excitation ($C_{lu} = C_{ul} = 0$) and complete redistribution over the line profile [$\phi_{ul}(\nu) = \phi_{lu}(\nu)$]. Physically, this means that emitted and absorbed photons are completely independent. Equation (4) then becomes:

$$n_l B_{lu} \int_0^\infty J_\nu \phi_{lu}(\nu) = n_u B_{ul} \int_0^\infty J_\nu \phi_{ul}(\nu) + n_u A_{ul}$$
$$\int_0^\infty [n_l B_{lu} J_\nu \phi_{lu}(\nu)] d\nu = \int_0^\infty [n_u B_{ul} J_\nu \phi_{lu}(\nu) + n_u A_{ul}] d\nu$$
$$n_l B_{lu} J_\nu \phi_{lu} = n_u B_{ul} J_\nu \phi_{lu} + n_u A_{ul}. \tag{5}$$

For a system in thermal equilibrium, the relative level populations follow the Boltzmann distribution:

$$\frac{n_u}{n_l} \equiv \frac{g_u}{g_l} \exp\left(-\frac{h\nu}{kT}\right), \tag{6}$$

and the radiation field J_ν is described by the Planck function $B_\nu(T)$:

$$B_\nu(T) \equiv \frac{2h\nu^3}{c^2} \left[\exp\left(\frac{h\nu}{kT}\right) - 1 \right]^{-1}. \tag{7}$$

Substituting equations (6) and (7) into equation (5) (which eliminates the line profile function ϕ_{lu}) yields, after some rearrangement:

$$\left(\frac{c^2}{2h\nu^3} A_{ul} - \frac{g_l}{g_u} B_{lu} \right) \left[\exp\left(\frac{h\nu}{kT}\right) - 1 \right] = \frac{g_l}{g_u} B_{lu} + B_{ul}, \tag{8}$$

which implies that:

$$g_l B_{lu} = g_u B_{ul} \tag{9}$$

$$A_{ul} = \frac{2h\nu^3}{c^2} B_{ul}. \tag{10}$$

For dipole emission, the spontaneous emission coefficient A_{ul} can be written in terms of the dipole matrix element $|\mu_{lu}|^2$ as:

$$A_{ul} \equiv \frac{64\pi^4\nu^3}{3hc^3}|\mu_{lu}|^2. \qquad (11)$$

3. RADIATIVE TRANSFER

The radiative transfer equation, ignoring scattering processes (such as those involving electrons or dust) is defined as follows (see Spitzer [1978] or Draine [2011] for details):

$$\frac{dI_\nu}{ds} = -\kappa_\nu I_\nu + j_\nu \qquad (12)$$

where $s \equiv$ path of propagation along the line of sight, $I_\nu \equiv$ specific intensity, and $\kappa_\nu \equiv$ absorption coefficient:

$$\kappa_\nu = \frac{h\nu}{4\pi}(n_l B_{lu} - n_u B_{ul})\phi_\nu \qquad (13)$$

$$\kappa_\nu = \frac{c^2}{8\pi\nu^2}\frac{g_u}{g_l}n_l A_{ul}\left(1 - \frac{g_l n_u}{g_u n_l}\right)\phi_\nu \qquad (14)$$

$j_\nu \equiv$ emission coefficient:

$$j_\nu = \frac{h\nu}{4\pi}A_{ul}n_u, \qquad (15)$$

Since we generally do not know what the propagation path is for our measured radiation, it is convenient to change independent variables from pathlength s to "optical depth" τ_ν, which is defined as:

$$d\tau_\nu \equiv \kappa_\nu ds, \qquad (16)$$

where we use the convention adopted by Draine (2011) that the radiation propagates in the direction of *increasing* optical depth.[1] Switching variables from s to τ_ν in our radiative transfer equation (eq. [12]) results in the following radiative transfer equation:

$$dI_\nu = S_\nu d\tau_\nu - I_\nu d\tau_\nu, \qquad (17)$$

where we define the *source function*, S_ν:

$$S_\nu \equiv \frac{j_\nu}{\kappa_\nu}. \qquad (18)$$

By multiplying both sides of equation (17) by the "integrating factor," e^{τ_ν}, we can integrate the radiative transfer equation

---

[1] Draine (2011) points out that Spitzer (1978) uses the opposite convention, that radiation propagates in the direction of *decreasing* optical depth.

from a starting point where $\tau_\nu = 0$ and $I_\nu = I_\nu(0)$ to find that:

$$e^{\tau_\nu}(dI_\nu + I_\nu d\tau_\nu) = e^{\tau_\nu}S_\nu d\tau_\nu$$

$$e^{\tau_\nu}I_\nu - I_\nu(0) = \int_0^{\tau'} S_\nu d\tau'$$

$$I_\nu = I_\nu(0)e^{-\tau_\nu} + \int_0^{\tau'}\exp[-(\tau_\nu - \tau')]S_\nu d\tau'. \qquad (19)$$

Equation (19) is a completely general solution to the equation of radiative transfer (again, assuming that scattering is neglected). It defines the intensity measured by the observer (I_ν) as the sum of the background intensity [$I_\nu(0)$] attenuated by the interstellar medium [$\exp(-\tau_\nu)$] plus the integrated emission ($S_\nu d\tau'$) attenuated by the effective absorption due to the interstellar medium between the point of emission and the observer $\{\exp[-(\tau_\nu - \tau')]\}$.

For an infinitely large medium, the radiation field would be defined as blackbody: $I_\nu = B_\nu$. We further assume that the medium through which the radiation is traveling is uniform at an excitation temperature, T_{ex}, defined as:

$$T_{ex} = \frac{h\nu/k}{\ln\left(\frac{n_l g_u}{n_u g_l}\right)}, \qquad (20)$$

where n is the density (cm^{-3}) in the upper (u) or lower (l) energy level for a transition with frequency ν. The source function S_ν is then equivalent to the Planck function at temperature T_{ex} (eq. [7]): $S_\nu = B_\nu(T_{ex})$. This condition is sometimes referred to as "local thermodynamic equilibrium" (LTE). Equation (19) becomes:

$$I_\nu = I_\nu(0)e^{-\tau_\nu} + \int_0^{\tau'}\exp[-(\tau_\nu - \tau')]B_\nu(T_{ex})d\tau'. \qquad (21)$$

If we further assume that T_{ex} is a constant, equation (21) becomes:

$$I_\nu = I_\nu(0)\exp(-\tau_\nu) + B_\nu(T_{ex})[1 - \exp(-\tau_\nu)]. \qquad (22)$$

Molecular spectral line measurements involve differencing the measured intensity toward a reference position that contains only background intensity from that measured toward a molecular line source position:

$$\Delta I_\nu \equiv I_\nu - I_\nu(0)$$
$$= I_\nu(0)\exp(-\tau_\nu) + B_\nu(T_{ex})[1 - \exp(-\tau_\nu)] - I_\nu(0)$$
$$= [B_\nu(T_{ex}) - B_\nu(T_{bg})][1 - \exp(-\tau_\nu)]. \qquad (23)$$

In many cases, the specific intensity I_v is replaced by the *Rayleigh–Jeans equivalent temperature*, which is the equivalent temperature of a black body at temperature T:

$$J_\nu(T) \equiv \frac{\frac{h\nu}{k}}{\exp(\frac{h\nu}{kT}) - 1}. \qquad (24)$$

If we further define the *radiation temperature* (T_R) as follows:

$$T_R \equiv \frac{c^2}{2k\nu^2} \Delta I_\nu, \qquad (25)$$

we can relate $B_\nu(T)$ and $J_\nu(T)$ as follows:

$$\frac{c^2}{2k\nu^2} B_\nu(T) = J_\nu(T). \qquad (26)$$

We can write our radiative transfer equation in a form which involves the observable *source radiation temperature* (T_R) derived from a differencing measurement:

$$T_R = f[J_\nu(T_{ex}) - J_\nu(T_{bg})][1 - \exp(-\tau_\nu)], \qquad (27)$$

where we have introduced an extra factor, f, which is the fraction of the spatial resolution of the measurement filled by the source (sometimes called the "filling factor"). See Ulich & Haas (1976) for a complete derivation of the source radiation temperature for the case of a single antenna position switched measurement.

4. COLUMN DENSITY

In order to derive physical conditions in the interstellar medium, it is often useful to measure the number of molecules per unit area along the line of sight. This quantity, called the "column density," is basically a first step to deriving basic physical quantities such as spatial density, molecular abundance, and kinetic temperature. Using the two-energy-level system defined above, we can express the column density as the number of molecules in energy level u integrated over the pathlength ds:

$$N_u \equiv \int n_u ds. \qquad (28)$$

Since we want to use our molecular spectral line measurements to calculate the molecular column density, which will ultimately involve the radiative transfer properties of the molecular spectral line measured, we can use the definition of the optical depth (eq. [16]), the definition of the absorption coefficient κ (eq. [14]), the Boltzmann equation for statistical equilibrium (eq. [6]), the definition of the spontaneous emission coefficient A_{ul} (eq. [11]), and our definition of the column density (eq. [28]) to relate τ_ν to the number of molecules in the upper energy state, N_u:

$$\tau_\nu = \frac{c^2}{8\pi\nu^2} \frac{g_u}{g_l} A_{ul}\phi_\nu \int ds' n_l(s') \left(1 - \frac{g_l n_u(s')}{g_u n_l(s')}\right)$$

$$= \frac{c^2}{8\pi\nu^2} \frac{g_u}{g_l} A_{ul}\phi_\nu N_l \left(1 - \frac{g_l N_u}{g_u N_l}\right)$$

$$= \frac{c^2}{8\pi\nu^2} \left[\exp\left(\frac{h\nu}{kT}\right) - 1\right] A_{ul}\phi_\nu N_u$$

$$= \frac{8\pi^3\nu|\mu_{lu}|^2}{3hc} \left[\exp\left(\frac{h\nu}{kT}\right) - 1\right]\phi_\nu N_u$$

$$\int \tau_\nu d\nu = \frac{8\pi^3\nu|\mu_{lu}|^2}{3hc} \left[\exp\left(\frac{h\nu}{kT}\right) - 1\right] N_u, \qquad (29)$$

where in the last step we have integrated over the line profile such that $\int \phi_\nu = 1$. Rearranging and converting our frequency axis to velocity ($dv/v = dv/c$) in equation (29), we get an expression for the column density of molecules in the upper transition state (N_u):

$$N_u = \frac{3h}{8\pi^3|\mu_{lu}|^2} \left[\exp\left(\frac{h\nu}{kT}\right) - 1\right]^{-1} \int \tau_\nu dv. \qquad (30)$$

At this point, we have our basic equation for the number of molecules in the upper energy state u of our two-level system. In order to relate this to the total molecular column density as measured by the intensity of a transition at frequency ν, we need to relate the number of molecules in the upper energy level u (N_u) to the total population of all energy levels in the molecule N_{tot}. Assuming detailed balance at a constant temperature defined by the excitation temperature T_{ex}, we can relate these two quantities as follows:

$$\frac{N_{tot}}{N_u} = \frac{Q_{rot}}{g_u} \exp\left(\frac{E_u}{kT_{ex}}\right), \qquad (31)$$

where we have introduced the "rotational partition function," Q_{rot}, a quantity that represents a statistical sum over all rotational energy levels in the molecule (see § 7) and g_u, the degeneracy of the energy level u. Substituting for N_u in equation (31), the total molecular column density becomes:

$$N_{tot} = \frac{3h}{8\pi^3|\mu_{lu}|^2} \frac{Q_{rot}}{g_u} \exp\left(\frac{E_u}{kT_{ex}}\right) \left[\exp\left(\frac{h\nu}{kT_{ex}}\right) - 1\right]^{-1} \int \tau_\nu dv. \qquad (32)$$

In the following, we show how to calculate the level degeneracy g_u (§ 5), the rotational partition function $Q_{rot} \equiv \sum_i g_i \exp(-E_i/kT)$ (§ 7), the dipole matrix element $|\mu_{lu}|^2$ and associated line strength S and dipole moment μ (such that $|\mu_{jk}|^2 \equiv S\mu^2$; § 8). For absorption lines where the integral of the optical depth over velocity may be derived from a spectrum, equation (32) may be used directly to determine the total column density. For emission lines, the integral over optical depth

is typically converted to an integrated intensity $\int T_R dv$ (see § 11). We derive several commonly used approximations to equation (32), including optically thin, optically thick, and the Rayleigh–Jeans approximation in § 11. We also evaluate the limitations of the common assumption that the molecular excitation temperature is constant (§ 12), summarize non-LTE models of the molecular column density (§ 13), and the distinction between beam-averaged and source-averaged column density (§ 14). We then close this discussion of molecular column density by working through several example calculations (§ 15). We also discuss some minor issues related to the assumed line profile function (Appendix A), the relationship between integrated fluxes and brightness temperatures (Appendix B), and the uncertainty associated with an integrated intensity measurement (Appendix C) in the appendices. In a calculation which utilizes the column density calculation formalism presented below, Appendix E describes the standard three-level model for low-temperature NH_3 excitation often used to derive the kinetic temperature from measurements of the (1,1) and (2,2) inversion transitions of that molecule.

5. DEGENERACIES

For rotational molecular transitions, the total degeneracy for an energy level of a transition is given by the product of rotational (g_J and g_K) and spin (g_I) degeneracies:

$$g_u \equiv g_J g_K g_I. \tag{33}$$

In the following, we derive the expressions for these three contributions to the degeneracy of a molecular energy level.

5.1. Rotational Degeneracy (g_J)

The rotational degeneracy due to the projection of the angular momentum on the spatial axis z, g_J, exists in all molecules and is given by:

$$g_J = 2J_u + 1. \tag{34}$$

5.2. K Degeneracy (g_K)

The K degeneracy (g_K) describes the degeneracy associated with the internal quantum number K in symmetric and asymmetric top molecules due to projections of the total angular momentum onto a molecular axis. Because of the opposite symmetry of the doubly degenerate levels for which $K \neq 0$, g_K is defined as follows:

$$g_K = 1 \quad \text{for } K = 0 \text{ and all linear and asymmetric top molecules} \tag{35}$$

$$g_K = 2 \quad \text{for } K \neq 0 \text{ in symmetric top molecules} \tag{36}$$

K-level doubling is due to the asymmetry in the molecule about the molecular axes and removes the K degeneracy in asymmetric top molecules.

5.3. Nuclear Spin Degeneracy (g_I)

The nuclear spin degeneracy, g_I, takes account of the statistical weights associated with identical nuclei in a nonlinear molecule with symmetry (which most nonlinear molecules have). For a molecule with *no symmetry or hyperfine splitting*, each rotational level will have a nuclear spin degeneracy given by:

$$g_n = \prod_i (2I_i + 1) = (2I + 1)^\sigma \tag{37}$$

$$g_I \equiv \frac{g_{\text{nuclear}}}{g_n}, \tag{38}$$

where I_i represents the spin of the ith nucleus, σ is the number of identical nuclei, and g_{nuclear} is given in Table 1 for two of the largest classes of molecules found in the interstellar medium: those with two (C_{2v} symmetry) and three (C_{3v} symmetry) identical nuclei.[2] Symmetry and hyperfine splitting changes g_n for all practical cases. Hyperfine splitting is covered elsewhere in this document, while symmetry considerations are well-covered by Gordy & Cook (1984; Chapter III.4). See also Turner (1991) for a general discussion applicable to the high-temperature limit. *Keep in mind that if you are only interested in studying one symmetry state (i.e., the para species) of a molecule, $g_I = 1$.* In the following, we list some examples of g_{nuclear} calculations for several molecules.

5.3.1. H_2CO *and* c-C_3H_2

Formaldehyde (H_2CO) is a (slightly; $\kappa = -0.96$; see eq. [45]) prolate (see § 6) asymmetric top molecule, while cyclopropenylidene (c-C_3H_2) is a cyclic (slightly; $\kappa = +0.69$) oblate (see § 6) asymmetric top molecule. Both have two opposing identical H (spin $= 1/2$) nuclei. The coordinate wavefunction is symmetric/asymmetric for K_{-1} even/odd, respectively. Therefore, from the two identical spin $1/2$ nuclei cases in Table 1:

$$g_{\text{nuclear}} = (2I + 1)I = 1 \quad \text{for } K_{-1} \text{ even} \tag{39}$$

$$g_{\text{nuclear}} = (2I + 1)(I + 1) = 3 \quad \text{for } K_{-1} \text{ odd} \tag{40}$$

---

[2] The number of symmetry states for a molecule are determined by the number of configurations within which the wavefunction of the molecule is unchanged with a rotation of π about a symmetry axis and a reflection of π through that symmetry plane. For a nice tutorial on molecular symmetry, see Stefan Immel's extensive discussion at http://csi.chemie.tu-darmstadt.de/ak/immel/tutorials/symmetry/index7.html.

TABLE 1
NUCLEAR STATISTICAL WEIGHT FACTORS FOR C_{2v} AND C_{3v} MOLECULES

Identical nuclei (σ)[a]	Spin	J	K[b]	$g_{nuclear}$
2	$\frac{1}{2}, \frac{3}{2}, \ldots$	Any	Even	$(2I+1)I$
2	$\frac{1}{2}, \frac{3}{2}, \ldots$	Any	Odd	$(2I+1)(I+1)$
2	$0,1,2,\ldots$	Any	Odd	$(2I+1)(I+1)$
2	$0,1,2,\ldots$	Any	Even	$(2I+1)I$
3	Any	Even or odd	$3n, \neq 0$	$\frac{1}{3}(2I+1)(4I^2+4I+3)$
3	Any	Even or odd	$\neq 3n$	$\frac{1}{3}(2I+1)(4I^2+4I)$

NOTE.—Derived from Gordy & Cook (1984), Tables 3.2 and 3.3.
[a] $g_I \equiv \frac{g_{nuclear}}{(2I+1)^\sigma}$
[b] Where n is an integer.

5.3.2. NH_3 *and* CH_3CN

Ammonia (NH_3) and acetonitrile (CH_3CN) are symmetric top molecules with three opposing identical H (spin = 1/2) nuclei. Therefore, from the three identical spin 1/2 nuclei cases in Table 1:

$$g_{nuclear} = \frac{1}{3}(2I+1)(4I^2+4I+3) = 4 \quad \text{for } K = 3n, \quad (41)$$

$$= \frac{1}{3}(2I+1)(4I^2+4I) = 2 \quad \text{for } K \neq 3n. \quad (42)$$

5.3.3. c-C_3H *and* SO_2

Cyclopropynylidyne (c-C_3H) is an oblate ($\kappa = +0.17$) asymmetric top molecule with two opposing identical carbon (spin = 0) nuclei, while SO_2 is a prolate ($\kappa = -0.94$) asymmetric top molecule with two opposing identical oxygen (spin = 0) nuclei. For both molecules, the coordinate wavefunction is symmetric/asymmetric for K_{-1} even/odd, respectively. Therefore, from the two identical spin 0 nuclei cases in Table 1:

$$g_{nuclear} = (2I+1)I = 0 \quad \text{for } K_{-1} \text{ even} \quad (43)$$

$$g_{nuclear} = (2I+1)(I+1) = 1 \quad \text{for } K_{-1} \text{ odd} \quad (44)$$

This indicates that half of the levels are missing (those for which K_{-1} is even).

6. SYMMETRY CONSIDERATIONS FOR ASYMMETRIC ROTOR MOLECULES

The symmetry of the total wavefunction ψ for a given rotational transition is determined by the product of the coordinate wavefunction $\psi_e \psi_v \psi_r$ and the nuclear spin wavefunction ψ_n. It is common to refer to a symmetric nuclear spin state as "ortho" and an antisymmetric nuclear spin state as "para." These wavefunctions are of two types: fermions and bosons. Table 2 lists the symmetries for the various wavefunctions in both cases for exchange of two identical nuclei.

Since an asymmetric top can be thought of as belonging to one of two limiting cases, prolate or oblate symmetric, we need to consider these two cases in the context of the coordinate wavefunction $\psi_e \psi_v \psi_r$

Limiting prolate: We consider the symmetry of the coordinate wavefunctions with respect to rotation of 180° about the axis of *least* moment of inertia. Since the coordinate wavefunction $\psi_e \psi_v \psi_r$ depends on this rotation angle ξ as $\exp(\pm iK_{-1}\xi)$, it is *symmetric when K_{-1} is even and antisymmetric when K_{-1} is odd*. H_2CO is a limiting prolate asymmetric top molecule (though it is only *slightly* asymmetric).

Limiting oblate: We consider the symmetry of the coordinate wavefunctions with respect to rotation of 180° about the axis of *greatest* moment of inertia. Since the coordinate wavefunction $\psi_e \psi_v \psi_r$ depends on this rotation angle ξ as $\exp(\pm iK_{+1}\xi)$, it is *symmetric when K_{+1} is even and antisymmetric when K_{+1} is odd*. NH_2D is a limiting oblate asymmetric top molecule.

The level of asymmetry in molecules is often described in terms of Ray's asymmetry parameter κ (Ray 1932):

$$\kappa \equiv \frac{2B - A - C}{A - C}, \quad (45)$$

where A, B, and C are constants which represent the three principle moments of inertia for an asymmetric rotor molecule (see Gordy & Cook [1984] for more information), usually expressed in megahertz (MHz). The limits to κ are:

TABLE 2
EIGENFUNCTION SYMMETRIES FOR EXCHANGE OF TWO IDENTICAL NUCLEI

Statistics	Spin (I)	Wavefunction[a]			$g_{nuclear}$
		Total (ψ)	Coordinate ($\psi_e \psi_v \psi_r$)	Spin (ψ_n)	
Fermi	$\frac{1}{2}, \frac{3}{2}, \ldots$	A	S	A	$(2I+1)I$
Fermi	$\frac{1}{2}, \frac{3}{2}, \ldots$	A	A	S	$(2I+1)(I+1)$
Bose	$0,1,2,\ldots$	S	S	S	$(2I+1)(I+1)$
Bose	$0,1,2,\ldots$	S	A	A	$(2I+1)I$

NOTE.—From Gordy & Cook (1984), Table 3.2.
[a] A = asymmetric; S = symmetric. For nuclear spin states asymmetric = "para," while symmetric = "ortho."

1. $B = A$: $\kappa = +1$ and the molecule is an oblate symmetric rotor

2. $B = C$: $\kappa = -1$ and the molecule is a prolate symmetric rotor

Taking a more general example, the rotational angular momentum constants for H_2CO are $A = 281970.37$ MHz, $B = 38835.42558$ MHz, and $C = 34005.73031$ MHz. Equation (45) then yields $\kappa \simeq -0.961$, which means that H_2CO is nearly a prolate symmetric rotor.

7. ROTATIONAL PARTITION FUNCTIONS (Q_{rot})

For a parcel of gas that exchanges energy with the ambient medium, statistical mechanics states that the partition function Q which describes the relative population of states in the gas is given by:

$$Q = \sum_i g_i \exp\left(-\frac{E_i}{kT}\right). \tag{46}$$

Following Gordy & Cook (1984; Chapter 3, § 3), the partition function for molecules in a gaseous state is a function of the electronic, vibrational, rotational, and nuclear spin states of the molecule. Assuming that there are no interactions between these states, the total partition function for the molecule can be expressed as the product of the partition functions of these four types of energy states:

$$Q = Q_e Q_v Q_r Q_n. \tag{47}$$

The ground electronic state of most molecules observed in the interstellar medium are stable, $^1\Sigma$ electronic states, although there are a few notable exceptions (i.e., OH $^2\Pi$, SO $^3\Sigma$, CN $^2\Sigma$, etc.). For these molecules $Q_e = 1$. For simplicity we will also assume that the molecules are in their ground vibrational state ($Q_v = 1$). This leaves us with rotational and nuclear partition functions comprising the total molecular partition function, which we can write as:

$$Q_{\text{rot}} \equiv Q_r Q_n$$
$$= \sum_{J,K,I} g_J g_K g_I \exp\left(-\frac{E_{JK}}{kT}\right), \tag{48}$$

where the degeneracies g_J, g_K, and g_I are described in §§ 5.1, 5.2, and 5.3, respectively. See Turner (1991) for a nice general discussion listing expressions for Q_{rot} in the high-temperature limit for a variety of molecules. In the following, we derive the rotational partition function Q_{rot} for linear, symmetric, and asymmetric rotor molecules.

7.1. Linear Molecule Rotational Partition Function

For linear molecules:

1. $g_J = 2J + 1$ (§ 5.1)
2. $g_K = 1$ (§ 5.2)
3. $g_I = 1$ (since linear molecules with allowed electric dipole transitions are polar and have no center of symmetry)

which implies that equation (48) becomes:

$$Q_{\text{rot}} = \sum_{J=0}^{\infty} (2J + 1) \exp\left(-\frac{E_J}{kT}\right). \tag{49}$$

The energy levels for a linear molecule can be described by a multiterm expansion as a function of $J(J+1)$ (Jennings et al. 1987):

$$E_J = h(B_0 J(J+1) - D_0 J^2(J+1)^2 + H_0 J^3(J+1)^3$$
$$- L_0 J^4(J+1)^4 + M_0 J^5(J+1)^5 + \ldots), \tag{50}$$

where B_0 is the rigid rotor rotation constant and D_0, H_0, L_0, and M_0 are the first-order through fourth-order centrifugal distortion constants for the molecule, respectively, all in megahertz (MHz). Using the rigid rotor approximation to the level energies, thus ignoring all terms other than those linear in $J(J+1)$, equation (50) becomes:

$$E_J = hB_0 J(J+1). \tag{51}$$

This allows us to approximate Q_{rot} for diatomic linear molecules as follows:

$$Q_{\text{rot}} \simeq \sum_{J=0}^{\infty} (2J+1) \exp\left(-\frac{hB_0 J(J+1)}{kT}\right)$$
$$\simeq \frac{kT}{hB_0} + \frac{1}{3} + \frac{1}{15}\left(\frac{hB_0}{kT}\right) + \frac{4}{315}\left(\frac{hB_0}{kT}\right)^2$$
$$+ \frac{1}{315}\left(\frac{hB_0}{kT}\right)^3 + \ldots \tag{52}$$

(from Gordy & Cook [1984], Chapter 3, equation [3.64], and McDowell [1988], where application of the Euler–MacLaurin summation formula has been used). This approximate form is good to $<1\%$ for $T > 2$ K (Fig. 1). This level of accuracy is maintained even if one includes only the first two terms in equation (52).

An alternate approximation for linear polyatomic molecules is derived by McDowell (1988):

$$Q_{\text{rot}} \simeq \frac{kT}{hB_0} \exp\left(\frac{hB_0}{3kT}\right), \tag{53}$$

which is reported to be good to 0.01% for $\frac{hB_0}{kT} \lesssim 0.2$ ($T > 13.7$ K for CO) and is good to better than 1% for $T > 3.5$ K (Fig. 1). Note that equation (53) reduces to equation (52) when expanded using a Taylor series.
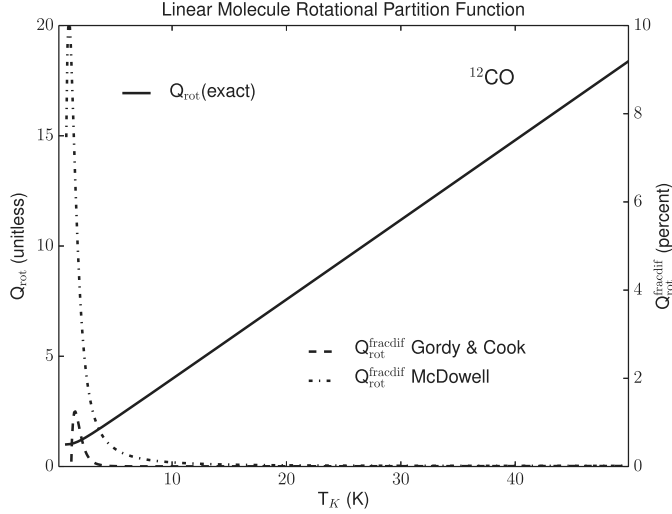
FIG. 1.—Rotational partition function calculations for CO using the lowest 51 levels of the molecule. Shown are (eq. [49]; *vertical scale on left*) and the percentage differences between Q_{rot} and the expansions of eq. (49) provided by eq. (52) (using terms to third-order in hB_0/kT) and eq. (53) (*vertical scale on right*).

7.2. Symmetric and Slightly Asymmetric Rotor Molecule Rotational Partition Function

For symmetric and asymmetric rotor molecules:

1. $g_J = 2J + 1$ (§ 5.1)
2. $g_K = 1$ for $K = 0$ and 2 for $K \neq 0$ in symmetric rotors (§ 5.2)
3. $g_K = 1$ for all K in asymmetric rotors
4. $g_I = \frac{g_{nuclear}}{(2I+1)^\sigma}$ (see Table 1)

which implies that equation (48) becomes:

$$Q_{rot} = \sum_{J=0}^{\infty} \sum_{K=-J}^{J} g_K g_I (2J+1) \exp\left(-\frac{E_{JK}}{kT}\right). \quad (54)$$

Like the energy levels for a linear molecule, the energy levels for a symmetric or slightly asymmetric[3] rotor molecule can be described by a multiterm expansion as a function of $J(J+1)$:

$$
\begin{aligned}
E_{JK} = h(&B_0 J(J+1) + s_0 K^2 + D_j J^2 (J+1)^2 \\
&+ D_{jk} J(J+1) K^2 + D_k K^4 + H_{jkk} J(J+1) K^4 \\
&+ H_{jjk} J^2 (J+1)^2 K^2 + H_{j6} J^3 (J+1)^3 + H_{k6} K^6 \\
&+ \ldots),
\end{aligned} \quad (55)
$$

where $s_0 \equiv A_0 - B_0$ for a prolate symmetric rotor molecule and $s_0 \equiv C_0 - B_0$ for an oblate symmetric rotor, and the other

---

[3] Slightly asymmetric rotor molecules are defined such that $B_0 \simeq C_0$. In equation (55) replace B with $\sqrt{B_0 C_0}$.

---

constants represent various terms in the centrifugal distortion of the molecule. All constants are in megahertz (MHz). For rigid symmetric or slightly asymmetric rotor molecules, using the rigid rotor approximation to the level energies:

$$E_{JK} = h[B_0 J(J+1) + s_0 K^2]. \quad (56)$$

From McDowell (1990), we can then approximate Q_{rot} for a symmetric or slightly asymmetric rotor molecule as follows:

$$
\begin{aligned}
Q_{rot} \simeq &\frac{\sqrt{m\pi}}{\sigma} \exp\left[\frac{hB_0(4-m)}{12kT}\right] \left(\frac{kT}{hB_0}\right)^{3/2} \\
&\times \left\{1 + \frac{1}{90}\left(\frac{hB_0(1-m)}{kT}\right)^2 + \ldots\right\},
\end{aligned} \quad (57)
$$

where

$$m = \frac{B_0}{A_0} \text{ for a prolate symmetric rotor molecule,}$$

$$= \frac{B_0}{C_0} \text{ for an oblate symmetric rotor molecule,}$$

$$= \frac{B_0^2}{A_0 C_0} \text{ for a slightly asymmetric rotor molecule}$$

(see Herzberg [1945]).

If we expand the exponential and take only up to first-order terms in the expansion in equation (57):

$$
\begin{aligned}
Q_{rot} &\simeq \frac{\sqrt{m\pi}}{\sigma} \left(1 + \frac{hB_0(4-m)}{12kT} + \ldots\right) \left(\frac{kT}{hB_0}\right)^{3/2} \\
&\simeq \frac{\sqrt{m\pi}}{\sigma} \left(\frac{kT}{hB_0}\right)^{3/2} \\
&\simeq \frac{1}{\sigma} \left[m\pi \left(\frac{kT}{hB_0}\right)^3\right]^{1/2},
\end{aligned} \quad (58)
$$

which is the equation for symmetric rotor partition functions quoted by Gordy & Cook (1984; Chapter 3, eqs. [3.68] and [3.69]). Figure 2 compares Q_{rot} calculated using equation (54) and the approximate forms given by equation (57) and equation (58) for NH_3. In this example, equation (57) is good to $\lesssim 20\%$ for $T_K > 10$ K and $\lesssim 0.25\%$ for $T_K > 50$ K, while equation (58) is much less accurate, good to $\lesssim 40\%$ for $T_K > 10$ K and $\lesssim 6\%$ for $T_K > 50$ K.

8. DIPOLE MOMENT MATRIX ELEMENTS ($|\mu_{jk}|^2$) AND LINE STRENGTHS (S)

The following discussion is derived from the excellent discussion given in Gordy & Cook (1984; Chapter II.6). A detailed discussion of line strengths for diatomic molecules can be found in Tatum (1986). Spectral transitions are induced by interaction
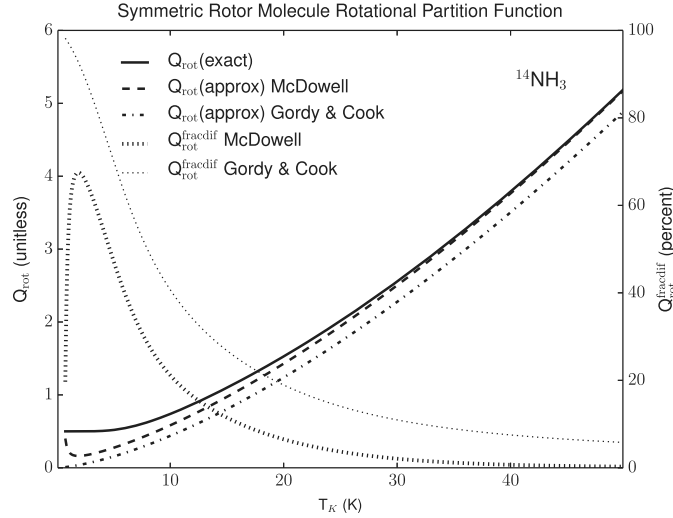
Symmetric Rotor Molecule Rotational Partition Function

$^{14}NH_3$

FIG. 2.—Rotational partition function calculations for NH_3 using the lowest 51 levels of the molecule. Shown are the exact summation for Q_{rot} (eq. [54]) and the approximate forms given by eqs. (57) and (58) (*vertical scale on left*). Shown also are the fractional percentage differences (*vertical scale on right*), given by $100\{[Q_{rot}(exact) - Q_{rot}(approx)]/Q_{rot}(exact)\}$, of these two approximations relative to Q_{rot} (eq. [54]).

of the electric or magnetic components of the radiation field in space with the electric or magnetic dipole components fixed in the rotating molecule. The strength of this interaction is called the *line strength* S. The matrix elements of the dipole moment with reference to the space-fixed axes (X, Y, Z) for the rotational eigenfunctions ψ_r can be written as follows:

$$\int \psi_r^* \mu_F \psi_r' d\tau = \sum_g \mu_g \int \psi_r^* \Phi_{Fg} \psi_r' d\tau, \qquad (59)$$

where Φ_{Fg} is the direction cosine between the space-fixed axes $F = (X, Y, Z)$ and the molecule-fixed axes $g = (x, y, z)$. The matrix elements required to calculate line strengths for linear and symmetric top molecules are known and can be evaluated in a straightforward manner, but these calculations are rather tedious because of the complex form of the eigenfunction. Using commutation rules between the angular momentum operators and the direction cosines Φ_{Fg}, Cross et al. (1944) derive the nonvanishing direction cosine matrix elements in the symmetric top representation (J, K, M):

$$\langle J, K, M | \Phi_{Fg} | J', K', M' \rangle$$
$$= \langle J | \Phi_{Fg} | J' \rangle \times \langle J, K | \Phi_{Fg} | J', K' \rangle \langle J, M | \Phi_{Fg} | J', M' \rangle, \qquad (60)$$

where M is the projection of the total angular momentum J on a fixed space axis. There are $2J + 1$ projections of M allowed. The dipole moment matrix element $|\mu_{lu}|^2$ can then be written as:

$$|\mu_{lu}|^2 = \sum_{F=X,Y,Z} \sum_{M'} |\langle J, K, M | \mu_F | J', K', M' \rangle|^2, \qquad (61)$$

where the sum over $g = x, y, z$ is contained in the expression for μ_F (eq. [59]). Table 3 lists the direction cosine matrix element factors in equation (60) for symmetric rotor and linear molecules. In the following, we give examples of the use of the matrix elements in line strength calculations.

9. LINEAR AND SYMMETRIC ROTOR LINE STRENGTHS

For all linear and most symmetric top molecules, the permanent dipole moment of the molecule lies completely along the axis of symmetry of the molecule ($\mu = \mu_z$). This general rule is only violated for the extremely-rare "accidentally symmetric top" molecule (where $I_x = I_y$). For all practical cases, then, equation (61) becomes:

$$|\mu_{lu}|^2 = \mu^2 \sum_{F=X,Y,Z} \sum_{M'} |\langle J, K, M | \Phi_{Fg} | J', K', M' \rangle|^2$$
$$= \mu^2 S, \qquad (62)$$

where we have defined the line strength S as:

$$S \equiv \sum_{F=X,Y,Z} \sum_{M'} |\langle J, K, M | \Phi_{Fg} | J', K', M' \rangle|^2. \qquad (63)$$

9.1. $(J, K) \rightarrow (J - 1, K)$ Transitions

Using the matrix element terms listed in the fourth column of Table 2 with the definition of the direction cosine matrix elements (eq. [60]), we can write the terms which make up equation (62) for the case $(J, K) \rightarrow (J - 1, K)^4$ as follows:

$$|\mu_{lu}|^2 = \mu^2 \left[\frac{(J^2 - K^2)^{1/2}}{J(4J^2 - 1)^{1/2}} \right] \left\{ (J^2 - M^2)^{1/2} \right.$$
$$\left. + \left(\frac{i \pm 1}{2} \right) [(J \mp M)(J \mp M - 1)]^{1/2} \right\}. \qquad (64)$$

Applying these terms to the dipole moment matrix element (eq. [61], which simply entails squaring each of the three terms in equation (64) and expanding the ± terms) and using the definition of $|\mu_{lu}|^2$ (eq. [63]):

$$S = \left[\frac{(J^2 - K^2)}{J^2(4J^2 - 1)} \right] [(J^2 - M^2)$$
$$+ \frac{1}{2} \{ (J - M)(J - M - 1) + (J + M)(J + M - 1) \}]. \qquad (65)$$

---

[4] Also referred to as "P-branch transitions."

Matrix element term	J' value		
	$J+1$	J	$J-1$
$\langle J|\Phi_{Fg}|J'\rangle$	$\{4(J+1)[(2J+1)(2J+3)]^{\frac{1}{2}}\}^{-1}$	$[4J(J+1)]^{-1}$	$[4J(4J^2+1)^{\frac{1}{2}}]^{-1}$
$\langle J,K|\Phi_{Fz}|J',K\rangle$	$2[(J+1)^2-K^2]^{\frac{1}{2}}$	$2K$	$-2(J^2-K^2)^{\frac{1}{2}}$
$\langle J,K|\Phi_{Fy}|J',K\pm1\rangle=\mp i\langle J,K|\Phi_{Fx}|J',K\pm1\rangle$	$\mp[(J\pm K+1)(J\pm K+2)]^{\frac{1}{2}}$	$[J(J+1)-K(K+1)]^{\frac{1}{2}}$	$\mp[(J\mp K)(J\mp K-1)]^{\frac{1}{2}}$
$\langle J,M|\Phi_{Zg}|J',M\rangle$	$2[(J+1)^2-M^2]^{\frac{1}{2}}$	$2M$	$-2(J^2-M^2)^{\frac{1}{2}}$
$\langle J,M|\Phi_{Yg}|J',M\pm1\rangle=\pm i\langle J,M|\Phi_{Xg}|J',M\pm1\rangle$	$\mp[(J\pm M+1)(J\pm M+2)]^{\frac{1}{2}}$	$[J(J+1)-M(M+1)]^{\frac{1}{2}}$	$\mp[(J\mp M)(J\mp M-1)]^{\frac{1}{2}}$

NOTES.—Derived from Gordy & Cook (1984), Table 2.1, which is itself derived from Cross et al. (1944). For linear molecules, set $K=0$ in the terms listed.

Reducing equation (65) results in the following for a symmetric top transition $(J,K)\to(J-1,K)$:

$$S=\frac{J^2-K^2}{J(2J+1)} \quad \text{for } (J,K)\to(J-1,K). \tag{66}$$

To derive the equation for a linear molecule transition $J\to J-1$, simply set $K=0$ in equation (66).

9.2. $(J,K)\to(J,K)$ Transitions

Using the matrix element terms listed in the fourth column of Table 3 with the definition of the direction cosine matrix elements (eq. [60]), we can write the terms which make-up equation (62) for the case $(J,K)\to(J,K)$[5] as follows:

$$|\mu_{lu}|^2=\mu^2\left[\frac{2K}{4J(J+1)}\right]\{2M\pm2[J(J+1)\\-M(M\pm1)]^{1/2}\}. \tag{67}$$

Applying these terms to the dipole moment matrix element (eq. [61]) and using the definition of $|\mu_{lu}|^2$ (§ 8):

$$S=\left[\frac{K^2}{4J^2(J+1)^2}\right]\{4M^2+2[J(J+1)-M(M+1)\\+J(J+1)-M(M-1)]\}. \tag{68}$$

Reducing equation (68) results in the following for a symmetric top transition $(J,K)\to(J,K)$:

$$S=\frac{K^2}{J(J+1)} \quad \text{for } (J,K)\to(J,K). \tag{69}$$

9.3. $(J,K)\to(J+1,K)$ Transitions

Using the matrix element terms listed in the second column of Table 3 with the definition of the direction cosine matrix elements (eq. [60]), we can write the terms which make up equation (62) for the case $(J,K)\to(J+1,K)$[6] as follows:

---

[5] Also referred to as "Q-branch transitions."
[6] Also referred to as "R-branch transitions."

$$|\mu_{lu}|^2=\mu^2\frac{[(J+1)^2-K^2]^{1/2}}{(J+1)[(2J+1)(2J+3)]^{1/2}}$$
$$\times\{[(J+1)^2-M^2]^{1/2}-\left(\frac{i\pm1}{2}\right)[(J\pm M+1)$$
$$\times(J\pm M+2)]^{1/2}\}. \tag{70}$$

Applying these terms to the dipole moment matrix element (eq. [61]), which simply entails squaring each of the three terms in eq. [70] and expanding the $\pm$ terms) and using the definition of $|\mu_{lu}|^2$ (eq. [63]):

$$S=\frac{[(J+1)^2-K^2]^{1/2}}{(J+1)[(2J+1)(2J+3)]^{1/2}}$$
$$\times\{(J+1)^2-M^2+\frac{1}{2}[(J+M+1)(J+M+2)$$
$$+(J-M+1)(J-M+2)]\}. \tag{71}$$

Reducing equation (71) results in the following for a symmetric top transition $(J,K)\to(J+1,K)$:

$$S=\frac{(J+1)^2-K^2}{(J+1)(2J+1)} \quad \text{for } (J,K)\to(J+1,K). \tag{72}$$

To derive the equation for a linear molecule transition $J\to J+1$, simply set $K=0$ in equation (72).

10. HYPERFINE STRUCTURE AND RELATIVE INTENSITIES

Hyperfine splitting in molecular spectra occurs when a nucleus in the molecule has nonzero nuclear spin. Hyperfine splitting is commonly observed in molecules that contain $^1\text{H}(I=1/2)$, $^2\text{D}(I=1)$, $^{13}\text{C}(I=1/2)$, $^{14}\text{N}(I=1)$, $^{15}\text{N}(I=1/2)$, $^{17}\text{O}(I=5/2)$, and $^{33}\text{S}(I=3/2)$ nuclei. For a molecule with a single coupling nucleus, the vector addition of angular momenta is used to define a new hyperfine quantum number, F, such that $\vec{F}=\vec{I}+\vec{J}$ is the total molecular angular momentum, where $\vec{I}$ and $\vec{J}$ are the nuclear spin and rotational angular momentum of the molecule respectively ($\vec{I}$ and $\vec{J}$ precess around $\vec{F}$). The allowed scalar values of $\vec{F}$ are given by

$$F = J + I, J + I - 1, \ldots, |J - I|. \tag{73}$$

Selection rules stipulate that $\Delta F = 0, \pm 1$ (but $F = 0$ cannot go to 0). For example, the ^{14}N nucleus in HCN is responsible for strong hyperfine coupling because the spin of ^{14}N is $I = 1$. Equation (73) shows that the $J = 0$ level remains unsplit ($F = 1$), the $J = 1$ level splits into a triplet ($F = 2, 1, 0$), and the $J = 2$ level also splits into a triplet ($F = 3, 2, 1$). The selection rule allows three hyperfine transitions from $J = 1 - 0$ and six hyperfine transitions from $J = 2 - 1$. Since $I = 1$ and the Clebsch–Gordon series (eq. [73]) terminates with $F = |J - I|$, all of the levels with $J > 2$ will also be split into triplets.

The relative strengths can be calculated by using irreducible tensor methods (see Gordy & Cook [1984], Chapter 15). We define the relative strength such that the sum of the relative strength, R_i, of all transitions from $F' \rightarrow F$ for a given $J' \rightarrow J$ are equal to one:

$$\sum_{F'F} R_i(J'F' \rightarrow JF) = 1. \tag{74}$$

The relative line strengths are calculated in terms of a $6 - j$ symbol,

$$R_i(J'F' \rightarrow JF) = \frac{(2F + 1)(2F' + 1)}{(2I + 1)} \begin{Bmatrix} I & F' & J' \\ 1 & J & F \end{Bmatrix}^2. \tag{75}$$

With the aid of $6 - j$ tables (Edmonds 1960), and the property that $6 - j$ symbols are invariant with permutation of the columns, we find the appropriate $6 - j$ symbol for each transition:[7]

$$\begin{Bmatrix} a & b & c \\ 1 & c-1 & b-1 \end{Bmatrix}^2 = \frac{s(s+1)(s-2a-1)(s-2a)}{(2b-1)2b(2b+1)(2c-1)2c(2c+1)}$$

$$\begin{Bmatrix} a & b & c \\ 1 & c-1 & b \end{Bmatrix}^2 = \frac{2(s+1)(s-2a)(s-2b)(s-2c+1)}{2b(2b+1)(2b+2)(2c-1)2c(2c+1)}$$

$$\begin{Bmatrix} a & b & c \\ 1 & c-1 & b+1 \end{Bmatrix}^2 = \frac{(s-2b-1)(s-2b)(s-2c+1)(s-2c+2)}{(2b+1)(2b+2)(2b+3)(2c-1)2c(2c+1)}$$

$$\begin{Bmatrix} a & b & c \\ 1 & c & b \end{Bmatrix}^2 = \frac{[2b(b+1)+2c(c+1)-2a(a+1)]^2}{2b(2b+1)(2b+2)2c(2c+1)(2c+2)}, \tag{76}$$

where $s = a + b + c$. For example, in the case of the $J = 1 - 0$ $F = 2 - 1$ transition of HC^{14}N, the first $6 - j$ symbol in equation (76) should be used with $a = I = 1$, $b = F' = 2$, and $c = J' = 1$.

The formalism above may be generalized when multiple coupling nuclei are present. By extension, an arbitrary number, n,

---

[7] Many online calculation tools are available that will calculate $6j$ symbols. For example, see http://www.svengato.com/sixj.html.

of coupling nuclei may be included in the nested vector addition of angular momenta (i.e., $\vec{F}_i = \vec{J} + \vec{I}_1$, $\vec{F}_2 = \vec{F}_1 + \vec{I}_2$, ..., $\vec{F} = \vec{F}_{n-1} + \vec{I}_n$), and the relative intensities can be calculated by multiplying the relative strength equation n times with appropriate quantum numbers for each step in the nested vector addition. For example, in the case of two coupling nuclei with unequal strength, such as the outer (I_1) and inner (I_2) ^{14}N of N$_2$H$^+$, the nested coupling scheme $\vec{F}_1 = \vec{J} + \vec{I}_1$ and $\vec{F} = \vec{F}_1 + \vec{I}_2$ is used. The relative strength of the hyperfine transitions is then given by

$$R_i(J'F_1'F' \rightarrow JF_1F) = \frac{(2F_1'+1)(2F_1+1)(2F'+1)(2F+1)}{(2I_1+1)(2I_2+1)}$$

$$\times \begin{Bmatrix} I_1 & F_1' & J' \\ 1 & J & F_1 \end{Bmatrix}^2 \begin{Bmatrix} I_2 & F' & F_1' \\ 1 & F_1 & F \end{Bmatrix}^2. \tag{77}$$

While we have specifically discussed hyperfine splitting from nuclei with unequal coupling in this section, the addition of vector angular momenta in quantum mechanics is a general problem and the formalism above may be extended to problems with equal coupling nuclei (i.e., H$_2$CO) or for fine-structure splitting (i.e., in molecules with electronic states with total electronic spin $S > 0$) with an appropriate mapping of the quantum numbers.

We end this section by noting an important caveat with regards the interpretation of the relative intensities of hyperfine transitions. Anomalies between observed hyperfine transition intensities and those predicted by the quantum mechanics described in this section have been observed (see Kwan & Scoville [1974], Guilloteau & Baudry [1981], Walmsley et al. [1982], Stutzki et al. [1984], Stutzki & Winnewisser [1985], Bachiller et al. [1997], Daniel et al. [2006], and Hily-Blant et al. [2010] for examples). These anomalies are likely due to spectral line overlap between hyperfine transitions and can result in non-LTE hyperfine ratios.

11. APPROXIMATIONS TO THE COLUMN DENSITY EQUATION

In the following, we derive several commonly used approximations to the column density equation (32): optically thin ($\tau \ll 1$), optically thin when in the Rayleigh–Jeans limit ($h\nu \ll kT_{ex}$), and optically thin when in the Rayleigh–Jeans limit and negligible background emission ($T_{bg} \ll T_{ex}$).

11.1. Optically Thin Approximation

If we assume that $\tau_\nu \ll 1$, the radiative transfer equation (eq. [27]) becomes:

$$T_R = f[J(T_{ex}) - J(T_{bg})]\tau, \tag{78}$$

and the column density equation (eq. [32]) becomes:

$$N_{tot}^{thin} = \left(\frac{3h}{8\pi^3 S\mu^2 R_i}\right)\left(\frac{Q_{rot}}{g_J g_K g_I}\right)\frac{\exp\left(\frac{E_u}{kT_{ex}}\right)}{\exp\left(\frac{h\nu}{kT_{ex}}\right)-1}$$
$$\times \int \frac{T_R dv}{f(J_\nu(T_{ex})-J_\nu(T_{bg}))}. \quad (79)$$

The $J_\nu(T_{ex}) - J_\nu(T_{bg})$ term may be removed from the integral because the Planck function does not vary substantially across the frequency extent of a typical spectral line. For example, if we take the CO $J = 1 - 0$ transition at 115 GHz, then for a spectral line with a full width zero intensity of 200 MHz (corresponding to an extent of 520 km s^{-1}), the fractional change in the Planck function across the spectral line is less than 0.3% for all excitation temperatures above the CMB. For most sources within the Milky Way Galaxy, the extent of a spectral line is an order of magnitude smaller and the corresponding change in the Planck function across the transition is also smaller. The fractional uncertainty in the Planck function increases as the frequency of the transition increases; however, even at 1 THz, the fractional uncertainty is still less than 3% for a 500 km s^{-1} wide transition. As a result, the $J_\nu(T_{ex}) - J_\nu(T_{bg})$ term is approximately constant in all realistic cases and the integral term in equation (79) reduces to just the integrated intensity of the spectral line:

$$N_{tot}^{thin} = \left(\frac{3h}{8\pi^3 S\mu^2 R_i}\right)\left(\frac{Q_{rot}}{g_J g_K g_I}\right)\frac{\exp\left(\frac{E_u}{kT_{ex}}\right)}{\exp\left(\frac{h\nu}{kT_{ex}}\right)-1}$$
$$\times \frac{1}{(J_\nu(T_{ex})-J_\nu(T_{bg}))}\int \frac{T_R dv}{f}. \quad (80)$$

11.2. Optically Thin with Rayleigh–Jeans Approximation

Assume that $\tau \ll 1$ and $h\nu \ll kT_{ex}$. This reduces the term in brackets in equation (32) to $h\nu/kT_{ex}$, $J_\nu(T)$ to T, and reduces the radiative transfer equation to that derived in equation (78). Equation (32) then reduces to

$$N_{tot}^{thin+RJ} = \left(\frac{3k}{8\pi^3 \nu S\mu^2 R_i}\right)\left(\frac{Q_{rot}}{g_J g_K g_I}\right)\exp\left(\frac{E_u}{kT_{ex}}\right)$$
$$\times \int \frac{T_R T_{ex} dv}{f(T_{ex}-T_{bg})}. \quad (81)$$

We test the validity of these approximations by comparing the ratio of equation (80) (N_{tot}^{thin}) to equation (81) ($N_{tot}^{thin+RJ}$) in Figure 3. The column density calculated from equation (80) is always less than the column density calculated from equation (81) in the Rayleigh–Jeans limit. Darker shading corresponds to worse agreement between the equations. For example,

the Rayleigh–Jeans approximation is a good approximation (less than 5% disagreement between equations) for the low-frequency (4.8 GHz) H_2CO K-doublet transition for all excitation temperatures. The Rayleigh–Jeans approximation is still a good approximation for the NH_3 inversion transitions [e.g., (1,1), (2,2), etc.] at 24 GHz with less than 10% disagreement between the equations for $T_{ex} > 5$ K. Rayleigh–Jeans failure is more apparent for transitions at millimeter and shorter wavelengths. For instance, the $C^{18}O$ $J = 1 - 0$ line at 109.7 GHz has more than 15% disagreement between the optically-thin and optically-thin plus Rayleigh–Jeans approximations for $T_{ex} < 9$ K that rapidly increases toward lower excitation temperatures. It is possible to use equation (81) at submillimeter wavelengths $\nu > 300$ GHz if the excitation temperature is large (i.e., less than 10% disagreement at 300 GHz if $T_{ex} > 26$ K); however, for most cases in dense regions of molecular clouds where the tracer is subthermally populated with low excitation temperatures, equation (80) should be used.

11.3. Optically Thin with Rayleigh–Jeans Approximation and Negligible Background

Assuming that the temperature of the background source (i.e., the cosmic microwave background radiation [CMB]) is
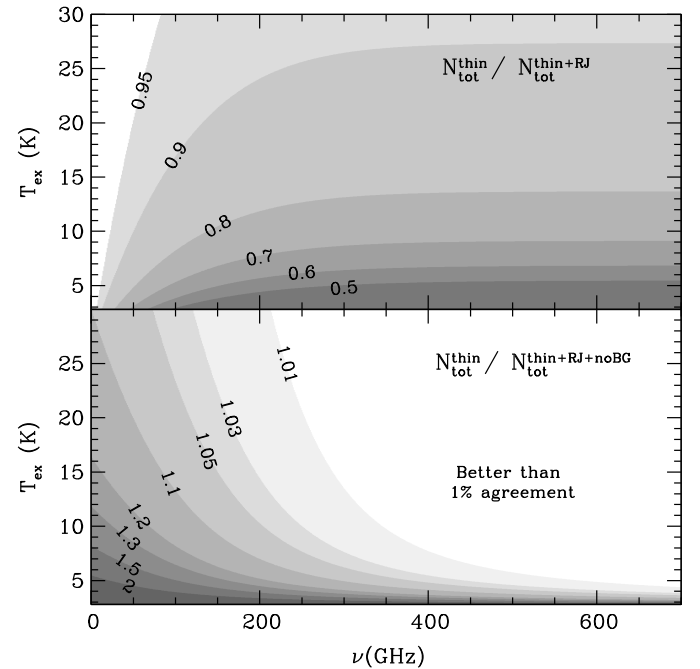
FIG. 3.—*Top*: Comparison of the molecular column density calculated assuming optically-thin (N_{tot}^{thin}; eq. [80]) and optically-thin within the Rayleigh–Jeans approximation ($N_{tot}^{thin+RJ}$; eq. [81]). *Bottom*: Comparison between molecular column density calculated assuming optically-thin and optically-thin within the Rayleigh–Jeans approximation and with the assumption of negligible background emission ($N_{tot}^{thin+RJ+noBG}$; eq. [82]).

small in comparison to the molecular excitation temperature ($T_{bg} \ll T_{ex}$), equation (81) becomes:

$$N_{\text{tot}}^{\text{thin}+RJ+noBG} = \left(\frac{3k}{8\pi^3 \nu S\mu^2 R_i}\right)\left(\frac{Q_{\text{rot}}}{g_J g_K g_I}\right)$$
$$\times \exp\left(\frac{E_u}{kT_{ex}}\right) \int \frac{T_R dv}{f}. \qquad (82)$$

We test when it is appropriate to use this approximation by comparing the column density calculated with equation (80) ($N_{\text{tot}}^{\text{thin}}$) versus equation (82) ($N_{tot}^{\text{thin}+RJ+noBG}$). The ratio of these two equations is given by $N_{\text{tot}}^{\text{thin}}/N_{\text{tot}}^{\text{thin}+RJ+noBG} = J_\nu(T_{ex})/[J_\nu(T_{ex}) - J_\nu(T_{bg})]$. Figure 3 shows contours of this ratio as a function of T_{ex} and the transition frequency. The general trend is such that the $thin + RJ + noBG$ approximation is poor for low frequencies and for low T_{ex}. At first, it seems counterintuitive that agreement between the two approximations would be better at high frequencies when failure of the Rayleigh–Jeans limit is more likely to occur (see § 11.2); however, ignoring the background term in equation (82) compensates for Rayleigh-Jeans failure. For high frequency and for $T_{ex} \gg T_{bg}$, the $J_\nu(T_{bg})$ term in the equation ratio becomes small such that $N_{\text{tot}}^{\text{thin}}/N_{\text{tot}}^{\text{thin}+RJ+noBG} \to 1$. The disagreement between the two equations is worse at smaller T_{ex}.

As a first example, we consider the NH_3 (1,1) lowest inversion transition at 23.7 GHz. At $T_{ex} = 10$ K, a common value found in NH_3 studies (see Rosolowsky et al. 2008), the $thin + RJ + noBG$ approximation results in a systematic 30% underestimate of the column density. At these frequencies, the CMB cannot be ignored. This result indicates that a column density expression with background (eq. [80] or [81]) should be used to calculate column densities from NH_3 (1,1) observations. In contrast, the $thin + RJ + noBG$ approximation is more applicable at higher frequencies. For the HCO^+ $J = 3 - 2$ transition at 267.5 GHz, equation (82) ($thin + RJ + noBG$ approximation) has better than 10% accuracy for $T_{ex} > 5.4$ K. Equation (82) may be used for submillimeter transitions ($\nu > 300$ GHz) unless the level populations for the transition are severely subthermally populated ($T_{ex} < 5$ K).

11.4. Not-Optically-Thin Approximation[8]

If we assume that $\tau_\nu \gtrsim 1$, we use the radiative transfer equation (eq. [27]) to solve for τ_ν:

$$\tau_\nu = -\ln\left[1 - \frac{T_R}{f[J(T_{ex}) - J(T_{bg})]}\right], \qquad (83)$$

---

[8] The condition $\tau \gtrsim 1$ is often somewhat erroneously referred to as "optically thick," while in fact the analysis presented in this section is appropriate for all conditions *excluding* $\tau \ll 1$.

and insert this expression for τ_ν in the column density equation (eq. [32]):

$$N_{\text{tot}}^{\text{thick}} = \left(\frac{3h}{8\pi^3 S\mu^2 R_i}\right)\left(\frac{Q_{\text{rot}}}{g_J g_K g_I}\right)\frac{\exp\left(\frac{E_u}{kT_{ex}}\right)}{\exp\left(\frac{h\nu}{kT_{ex}}\right) - 1}$$
$$\times \int -\ln\left[1 - \frac{T_R}{f[J(T_{ex}) - J(T_{bg})]}\right] dv. \qquad (84)$$

Note that equation (84) is quite general, applicable to all values of ν, τ, T_{ex}, T_{bg}, and T_R. Furthermore, one can derive a simple relationship between the column density derived assuming $\tau \ll 1$ and those derived assuming $\tau \nless 1$ by noting that one can write $N_{\text{tot}}^{\text{thin}}$ (eq. [80]) using the radiative transfer equation (eq. [27]) as follows:

$$N_{\text{tot}}^{\text{thin}} = \left(\frac{3h}{8\pi^3 S\mu^2 R_i}\right)\left(\frac{Q_{\text{rot}}}{g_J g_K g_I}\right)\frac{\exp\left(\frac{E_u}{kT_{ex}}\right)}{\exp\left(\frac{h\nu}{kT_{ex}}\right) - 1}$$
$$\times \int (1 - \exp(-\tau)) dv. \qquad (85)$$

Therefore, a column density calculated assuming $\tau \ll 1$ is related to a column density calculated more generally by the following:

$$N_{\text{tot}} = N_{\text{tot}}^{\text{thin}} \frac{\tau}{1 - \exp(-\tau)}. \qquad (86)$$

The factor $\tau/(1 - \exp(-\tau))$ is the "optical depth correction factor" derived by Goldsmith & Langer (1999). Note that equation (86) also applies to the approximation cases $h\nu \ll kT_{ex}$ (§ 11.2) and $T_{bg} \ll T_{ex}$ (11.3).

12. THE CONSEQUENCES OF ASSUMING A CONSTANT EXCITATION TEMPERATURE

The calculation of column density requires a determination of the gas excitation temperature (eq. [20]). The excitation temperature is a very general concept that describes an energy density (in units of temperature), whether kinetic, radiative, rotational, vibrational, spin, etc.

Since molecules are fundamentally multilevel systems, an excitation temperature may be defined for each transition allowed via electric dipole (or magnetic dipole or electric quadrupole) selection rules.[9] Most molecules (in particular, dense gas tracers) in the ISM are in non-LTE with different gas excitation temperatures for different transitions. However, to simplify the problem of calculating the total molecular column density from

---

[9] You can also define an "excitation temperature" between levels which are not radiatively coupled—e.g., the (1,1) and (2,2) inversion states of NH_3. This is usually called a rotation temperature T_{rot}.

a single transition, the constant excitation temperature approximation (CTEX) is usually assumed where all transitions have the same excitation temperature

$$T_{ex} = T_{ex}^{\mathrm{CTEX}} \forall \; u \to l. \tag{87}$$

The optically thin column densities using equation (80) are shown in Figure 4 for the three lowest-energy transitions of the HCO^+ molecule that are observable from the ground in atmospheric windows. Note that the column density equation diverges for $T_{ex}^{\mathrm{CTEX}} \to 2.735$ K due to the $J_\nu(T_{ex}) - J_\nu(T_{bg})$ term in the denominator. This divergence has the consequence that as the level populations approach equilibrium with the CMB, it becomes more difficult to accurately determine the column density. The plotted curves show N_{thin}/I or the column density in the optically thin limit for an integrated intensity of 1 K km s^{-1}. These curves should be multiplied by the observed integrated intensity and corrected for any optical depth effects by $\tau/[1 - \exp(-\tau)]$. The $1-0$ transition is the least sensitive transition to changes in the excitation temperature above 3 K with a minimum at $T_{ex}^{\mathrm{CTEX}} = 7.46$ K. As a result, the difference between assuming an excitation temperature between 5 K and 10 K results in a less than 10% uncertainty in the calculated column density assuming CTEX. This statement is in general true for the 3 mm transitions of several famous dense gas tracers such as HCO^+, HCN, N_2H^+, and CS. If a lower limit to the column density is desirable, then the column density can be calculated at the excitation temperature of the minimum excitation temperature curve (e.g., $N_{\mathrm{thin}}/I > 1.03 \times 10^{12}$ cm^{-2}/Kkms^{-1} for the HCO^+ $J = 1 - 0$ transition at $T_{ex}^{\mathrm{CTEX}} = 7.46$ K).

Estimating the total column density from higher energy transitions is more uncertain for low excitation temperatures. Unfortunately, this situation does occur in observations of dense cores in the ISM where the dense gas tracer is typically both optically thick and very subthermally populated (see Shirley et al. 2013). For the HCO^+ $J = 4 - 3$ transition, the uncertainty in the total column density calculation between assuming an excitation temperature of 5 K versus 10 K is a factor of 40! The $J = 4 - 3$ curve does not reach its minimum until $T_{ex}^{\mathrm{CTEX}} = 43.55$ K, close to the energy of the $J = 4$ level above ground ($E_u/k = 42.80$ K). It is therefore advisable to observe transitions with E_u/k that are comparable to the typical excitation temperature to minimize this uncertainty.

Proper estimation of the gas excitation temperature usually requires observations of multiple transitions coupled with modeling of the statistical equilibrium and radiative transfer. In general, the excitation temperature is a sigmoid function that varies between the background radiation temperature at low density and the gas kinetic temperature at high density. At low gas densities, collisions are not as important for setting the level populations as interaction with the background radiation field and the excitation temperature equilibrates with the radiation temperature. At high gas densities, collisions dominate
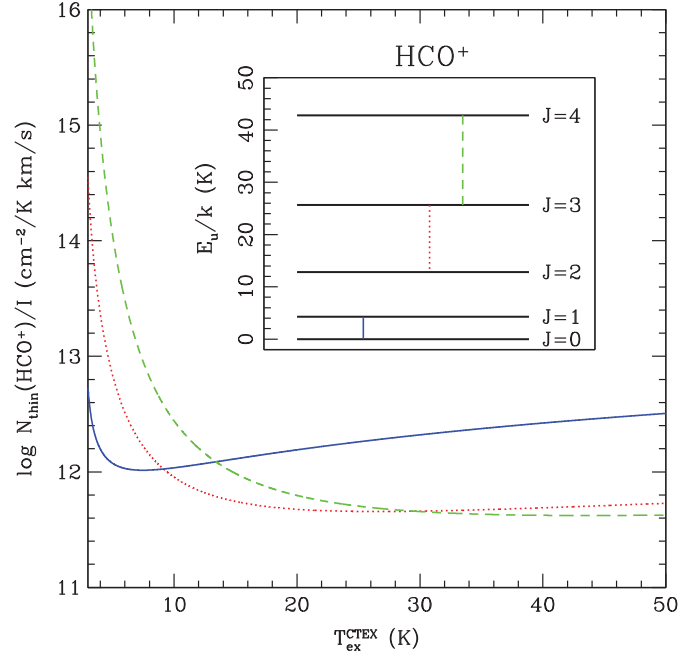

FIG. 4.—The optically thin column density at 1 K km s^{-1} for transitions of HCO^+. The $J = 1 - 0$ (*blue solid line*), $J = 3 - 2$ (*red dotted line*), and $J = 4 - 3$ (*green dashed line*) are plotted for different excitation temperatures in the CTEX approximation. The inset shows the energy level diagram for the lowest five energy levels of HCO^+ and the three transitions easily observable from ground-based observatories.

in setting the level populations and the excitation temperature equilibrates to the gas kinetic temperature of the dominant collisional partner. A transition is said to be "thermalized" if T_{ex} is equal to T_K. Subthermal excitation indicates that T_{ex} is less than T_K. In the general case of non-LTE in the ISM, it is possible that some transitions for a particular molecule may be thermalized (i.e., CO $J = 1 - 0$), while higher energy levels are subthermally populated (i.e., CO $J = 6 - 5$). Strong non-LTE effects are also observed in some cases (i.e., masers where naturally occurring population inversions can occur). Most molecular transitions of dense gas tracers observed in the ISM are subthermally populated.

Multilevel effects can cause departures from the sigmoid shape. For example, a bottleneck due to longer rates of spontaneous decay, $A_{ul} \sim \nu^3$, for low-J transitions can cause superthermal excitation in the $J = 1 - 0$ transition where, over a narrow range of densities, $T_{ex} > T_K$. A full discussion of multilevel statistical equilibrium with radiative transfer is beyond the scope of this tutorial. There are situations where the excitation temperature can be directly estimated from the observations. If it is known that the line is very optically thick, then the $(1 - e^{-\tau})$ term in the radiative transfer equation (eq. [27]) approaches 1, and the excitation temperature may be solved analytically with an assumption of the gas filling factor:

$$T_{ex}^{\mathrm{obs}} = \frac{h\nu/k}{\ln\left(1 + \frac{h\nu/k}{T_R/f + J_\nu(T_{\mathrm{cmb}})}\right)} \quad (\text{if } \tau \gg 1). \quad (88)$$

Molecular line ratios of well-resolved hyperfine transitions or ratios of isotopologues may be used to determine the optical depth in a line by taking ratios of equation (27) (see Appendix D), although these methods usually assume that the excitation temperature in each hyperfine line or among different isotopologue transitions are the same which may not always be true.

Figure 5 shows the dependence of equation (27) on the filling fraction by plotting the ratio of the excitation temperature at a filling fraction, f, divided by the excitation temperature with a filling fraction of $f = 1$ (the usual assumption when filling fraction is unknown). For intense spectral lines $T_R > 1$ K, calculation of T_{ex} from equation (27) is very sensitive to the gas filling fraction. For a line with $T_R = 1$ K, T_{ex} is 28% larger for $f = 0.5$. The value of $T_{ex}(f)$ quickly increases toward lower gas filling fractions. The dependence on gas filling fraction is steeper for brighter lines and flatter for weaker lines. The curves plotted in Figure 5 are not a strong function of the wavelength for transitions with $\lambda > 1$ cm.

If the line is optically thin, then it is not possible to determine the excitation temperature from a single transition as the observed line temperature, T_R, is degenerate with excitation
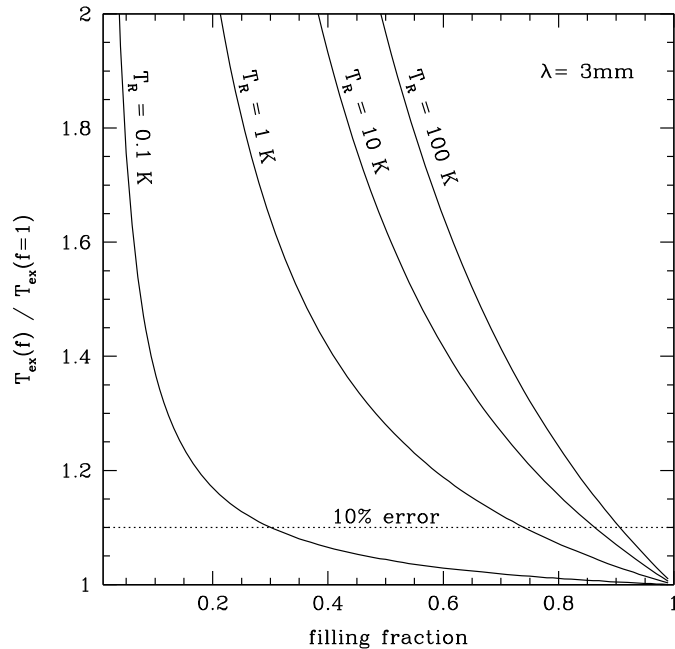

FIG. 5.—The ratio of the excitation temperature at a given gas filling fraction compared to the excitation temperature calculated assuming a gas filling fraction $f = 1$. The four curves correspond to spectral lines with $T_R = 0.1, 1, 10, 100$ K. The curves are calculated for a transition at 3 mm. The curves are a weak function of the transition frequency. The *horizontal dashed line* correspond to an error in T_{ex} of 10% compared to the $f = 1$ assumption.

temperature, optical depth, and filling fraction. However, in this case, the excitation temperature can still be estimated from multiple transitions using a rotation diagram. A detailed discussion of the limits of the CTEX approximation for HCO$^+$ observations may be found in Shirley et al. (2013).

13. NON-LTE APPROACHES TO THE DERIVATION OF MOLECULAR COLUMN DENSITY

Although beyond the scope of this tutorial, we should mention that there are a number of non-LTE approaches to the solution of the coupled multilevel statistical equilibrium and radiative transfer equations. These model-based solutions normally rely on the measurements of a number of molecular spectral lines from a given species to constrain the physical conditions within the dense gas environment under study. If one is interested in the global physical conditions within a molecular cloud, the radiative transfer solution for these models is simplified greatly by the introduction of a geometrically averaged escape probability (usually denoted by β). A number of escape probability expressions which depend upon the assumed molecular cloud geometry and global velocity field can be used in these global cloud models (see van der Tak et al. [2007] for an excellent discussion). One of the most popular of these non-LTE escape probability models incorporates the large velocity gradient (LVG) approximation (Sobolev 1960) to the solution of the radiative transfer and statistical equilibrium equations. At the heart of the LVG approximation is the assumption that photons which are emitted within the modeled molecular cloud escape quickly from the cloud due to the large velocity gradient (often assumed to be a result of cloud collapse). As described in Mangum & Wootten (1993) and van der Tak et al. (2007), in the LVG approximation the escape probability is given by $\beta = (1 - e^{-\tau})/\tau$ within a uniform collapsing spherical geometry. The molecular cloud is assumed to have uniform volume density, kinetic temperature, and molecular column density. Inputs to an LVG model include a specification of the molecular spectrum and collisional excitation rates involving the primary collision partner in the molecular cloud (usually assumed to be H$_2$) and the molecular species under study. Although the LVG approximation entails the use of a rather simplified uniform physical model, it often produces plausible physical conditions for environments where the transitions used to constrain the model are not too optically thick.

Other non-LTE approaches include the generalized escape probability code *RADEX* (van der Tak et al. 2007), microturbulent velocity models (Leung & Liszt 1976), and Monte Carlo approaches (Brinch & Hogerheijde 2010). In the microturbulent model solution, the molecular cloud is assumed to have a power-law distribution in volume density and kinetic temperature with a line profile that is produced due to a combination of thermal and turbulent motions. The radiative transfer equation is iteratively solved using a quasi-diffusion method. Monte Carlo models are generalized solutions to the radiative transfer in

molecular clouds which incorporate up to three dimensions of arbitrarily complex structure. This complex structure is organized into a grid of cells with uniform volume density, kinetic temperature, and molecular abundance. By ray tracing along random paths through this grid, the radiative transfer equation is iteratively solved.

Even though non-LTE approaches result in a more accurate representation of the physical conditions in a molecular cloud, they must be constrained by multiple molecular spectral line measurements from a given molecular species. Non-LTE models also require knowledge of the collisional excitation rates for the molecular species under study. Collisional excitation rates for a wide variety of molecules have been calculated (see, e.g., the Leiden Atomic and Molecular Database [LAMDA]; Schöier et al. [2005]). In general, though, limitations to their accuracy and kinetic temperature range can result in added uncertainty in non-LTE modeling of radiative transfer. Due to these limitations, LTE calculations of the molecular column density are often satisfactory with limited measurements.

14. BEAM-AVERAGED VERSUS SOURCE-AVERAGED COLUMN DENSITY

An aspect of the calculation of molecular column density from a spectral line measurement that is often overlooked is the difference between beam-averaged and source-averaged measurements. Beam-averaged molecular column densities are derived from spectral line measurements with a defined spatial resolution element (a radio telescope "beam" θ_{beam}). Without an understanding of the actual spatial extent of the measured emission (i.e., $\theta_{\text{beam}} > \theta_{\text{source}}$), one normally assumes that it is simply averaged over the beam of the measurement, or "beam-averaged." For measurements which resolve the spatial extent of emission (i.e., $\theta_{\text{beam}} < \theta_{\text{source}}$), spectral line measurements measured over a source, usually considered "extended," result in "source-averaged" molecular column densities.

15. MOLECULAR COLUMN DENSITY CALCULATION EXAMPLES

In the following, we describe in detail some illustrative calculations of the molecular column density. These example molecules were chosen for their commonality ($C^{18}O$ is an abundant, though often optically thin, isotopomer of CO), relatively simple hyperfine structure ($C^{17}O$), somewhat more complex hyperfine structure (N_2H^+), or general usage as kinetic temperature (NH_3) or volume density (H_2CO) probes. In these examples, we adopt the more conventional notation for a generic (emission or absorption) transition, i.e., "$J = 1 - 0$," instead of the more explicit (and somewhat less convenient) "$J = 1 \rightarrow 0$" notation. We also address a common point of confusion for students learning this material and its reliance on CGS (centimeter–gram–second) units. For the calculations presented below, dipole moments are quoted in the CGS unit "debye," which is equal to 10^{-18} esu

(electrostatic units). A good source for molecular dipole moments (μ) and rotational constants (i.e., A_0, B_0, C_0) is the Jet Propulsion Laboratory (JPL) Molecular Spectroscopy database and spectral line catalog (Pickett et al. 1998).[10]

15.1. $C^{18}O$

To derive the column density for $C^{18}O$ from a measurement of its $J = 1 - 0$ transition, we use the general equation for molecular column density (eq. [32]) with the following properties of the $C^{18}O$ $J = 1 - 0$ transition:

$$S = \frac{J_u}{2J_u + 1}$$

$$\mu = 0.1098 \text{ Debye} = 1.098 \times 10^{-19} \text{ esu}$$

$$B_0 = 57635.96 \text{ MHz}$$

$$g_J = 2J_u + 1$$

$$g_K = 1 \text{ (for linear molecules)}$$

$$g_I = 1 \text{ (for linear molecules)}$$

$$Q_{\text{rot}} \simeq \frac{kT}{hB} + \frac{1}{3} \text{ (eq.52)}$$

$$\simeq 0.38(T + 0.88)$$

$$E_u = 5.27 \text{ K}$$

$$\nu = 109.782182 \text{ GHz}$$

which leads to:

$$N_{\text{tot}}(C^{18}O) = \frac{3h}{8\pi^3\mu^2 J_u R_i} \left(\frac{kT_{ex}}{hB} + \frac{1}{3} \right) \exp\left(\frac{E_u}{kT_{ex}} \right)$$
$$\times \left[\exp\left(\frac{h\nu}{kT_{ex}} \right) - 1 \right]^{-1} \int \tau_\nu dv. \qquad (89)$$

Assuming that the emission is optically thin ($\tau_\nu \ll 1$; eq. [80]), equation (89) becomes:

$$N_{\text{tot}}(C^{18}O) = \frac{4.79 \times 10^{13}(T_{ex} + 0.88) \exp\left(\frac{5.27}{T_{ex}}\right)}{\exp\left(\frac{5.27}{T_{ex}}\right) - 1}$$
$$\times \left[\frac{T_B \Delta v(\text{km/s})}{f(J_\nu(T_{ex}) - J_\nu(T_{bg}))} \right] \text{cm}^{-2}. \qquad (90)$$

If we are using integrated fluxes ($S_\nu \Delta v$) instead of integrated brightness temperatures, we use equation (B2) (see Appendix B), with the assumption that $\tau \ll 1$:

---

[10] Available online at http://spec.jpl.nasa.gov (use the "catalog directory with links" to access dipole moment and molecular constants information).

$$N_{\text{tot}}(\text{C}^{18}\text{O}) = \frac{3c^2}{16\pi^3\Omega_s S\mu^2\nu^3}\left(\frac{Q_{\text{rot}}}{g_J g_K g_I}\right)\exp\left(\frac{E_u}{kT}\right)\int S_\nu \Delta v$$

$$= \frac{4.86\times10^{15}(T_{ex}+0.88)}{\theta_{\text{maj}}(\text{asec})\theta_{\text{min}}(\text{asec})}\frac{\exp(\frac{5.27}{T_{ex}})}{\exp(\frac{5.27}{T_{ex}})-1}$$

$$\times \left[\frac{S_\nu(Jy)\Delta v(\text{km/s})}{f(J_\nu(T_{ex})-J_\nu(T_{bg}))Z}\right]\text{cm}^{-2}. \quad (91)$$

where we have assumed a Gaussian source ($\Omega_s = 1.133\theta_{\text{maj}}\theta_{\text{min}}$ with θ_{maj} and θ_{min} the major and minor source diameters (in arcseconds).

15.2. C^{17}O

C^{17}O is a linear molecule with hyperfine structure due to interaction with the electric quadrupole moment of the ^{17}O($I=5/2$) nucleus. Using the selection rule:

$$F = J+I, J+I-1, J+I-2, ..., |J-I|,$$

we find that each J-level is split into the hyperfine levels indicated in Table 4 (for the first five J-levels). Since the selection rules for the single-spin coupling case is $\Delta F = 0, \pm1$, and $\Delta J = \pm1$, there are 3, 9, and 14 allowed hyperfine transitions for the $J=1-0$, $J=2-1$, and $J=3-2$ transitions, respectively. Figure 6 shows the energy level structure for the $J=1-0$ and $J=2-1$ transitions.

We can calculate the relative hyperfine intensities (R_i) for the $J=1-0$ and $J=2-1$ transitions using the formalism derived in § 10. Using the formalism described in § 10, we can derive the relevant R_i for the electric quadrupole hyperfine coupling cases [$R_i(F, J)$, $I=5/2$; Table 5]. Figure 7 shows the synthetic spectra for the C^{17}O $J=1-0$ and $J=2-1$ transitions.

To derive the column density for C^{17}O from a measurement of its $J=1-0$ transition we use the general equation for molecular column density (eq. [32]) with the following properties of the C^{17}O $J=1-0$ $F=(5/2)-(5/2)$ transition:

$$S = \frac{J_u}{2J_u+1}$$

$$\mu = 0.11032 \text{ Debye} = 1.1032\times10^{-19} \text{ esu}$$

$$B_0 = 56179.9911 \text{ MHz}$$

TABLE 4

ALLOWED C^{17}O HYPERFINE ENERGY LEVELS

J	Number of energy levels	Allowed F
0	1	$\frac{5}{2}$
1	3	$\frac{7}{2},\frac{5}{2},\frac{3}{2}$
2	5	$\frac{9}{2},\frac{7}{2},\frac{5}{2},\frac{3}{2},\frac{1}{2}$
3	6	$\frac{11}{2},\frac{9}{2},\frac{7}{2},\frac{5}{2},\frac{3}{2},\frac{1}{2}$
4	7	$\frac{13}{2},\frac{11}{2},\frac{9}{2},\frac{7}{2},\frac{5}{2},\frac{3}{2},\frac{1}{2}$
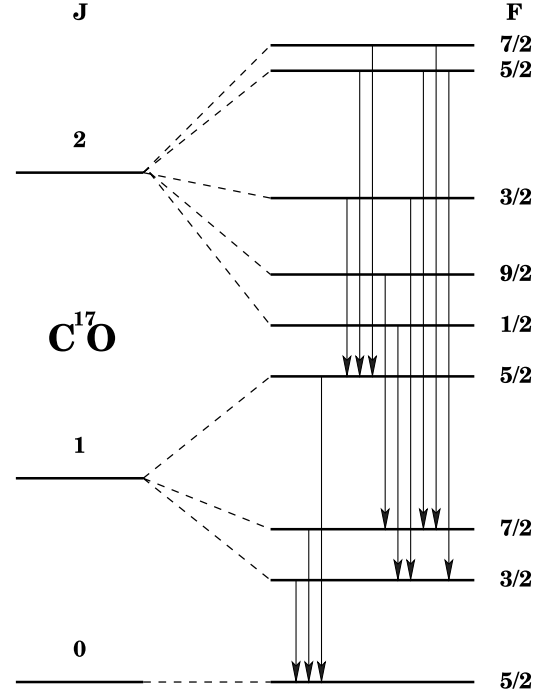
FIG. 6.—Electric quadrupole hyperfine energy level structure for the $J=0,1$, and to levels of C^{17}O. Note that the three ($J=1-0$) and nine ($J=2-1$) allowed transitions are marked with arrows ordered by increasing frequency from left to right.

$$g_J = 2J_u + 1$$

$$g_K = 1 \text{ (for linear molecules)}$$

$$g_I = 1 \text{ (for linear molecules)}$$

$$Q_{\text{rot}} \simeq \frac{kT}{hB} + \frac{1}{3} \text{ (eq.52)}$$

$$\simeq 0.37(T+0.90)$$

$$E_u = 5.39 \text{ K}$$

$$R_i = \frac{3}{9}$$

which leads to:

$$N_{\text{tot}}(\text{C}^{17}\text{O}) = \frac{3h}{8\pi^3\mu^2 J_u R_i}\left(\frac{kT_{ex}}{hB}+\frac{1}{3}\right)\exp\left(\frac{E_u}{kT_{ex}}\right)$$

$$\times \left[\exp\left(\frac{h\nu}{kT_{ex}}\right)-1\right]^{-1}\int \tau_\nu dv. \quad (92)$$

Assuming that the emission is optically thin ($\tau_\nu \ll 1$; eq. [80]), equation (92) becomes:

TABLE 5
HYPERFINE INTENSITIES FOR $C^{17}O$ $J = 1 - 0$ AND $J = 2 - 1$

$F' \to F$	$J' \to J$	a	b	c	$\frac{(2F'+1)(2F+1)}{(2I+1)}$	$\Delta\nu$ [a] (kHz)	6j	$R_i(F,J)$
$(\frac{3}{2}, \frac{5}{2})$	$(1,0)$	$\frac{5}{2}$	0	$\frac{5}{2}$	4	-501	$-\frac{1}{3\sqrt{2}}$	$\frac{2}{9}$
$(\frac{7}{2}, \frac{5}{2})$	$(1,0)$	$\frac{5}{2}$	1	$\frac{7}{2}$	8	-293	$-\frac{1}{3\sqrt{2}}$	$\frac{4}{9}$
$(\frac{5}{2}, \frac{5}{2})$	$(1,0)$	$\frac{5}{2}$	$\frac{5}{2}$	1	6	$+724$	$\frac{1}{3\sqrt{2}}$	$\frac{3}{9}$
$(\frac{3}{2}, \frac{5}{2})$	$(2,1)$	$\frac{5}{2}$	1	$\frac{5}{2}$	4	-867	$\frac{1}{10}$	$\frac{1}{25}$
$(\frac{5}{2}, \frac{5}{2})$	$(2,1)$	$\frac{5}{2}$	$\frac{5}{2}$	2	6	-323	$-\frac{4\sqrt{2}}{15\sqrt{7}}$	$\frac{64}{525}$
$(\frac{7}{2}, \frac{5}{2})$	$(2,1)$	$\frac{5}{2}$	2	$\frac{7}{2}$	8	-213	$\frac{\sqrt{3}}{2\sqrt{35}}$	$\frac{6}{35}$
$(\frac{9}{2}, \frac{7}{2})$	$(2,1)$	$\frac{5}{2}$	2	$\frac{9}{2}$	$\frac{40}{3}$	-169	$-\frac{1}{2\sqrt{10}}$	$\frac{1}{3}$
$(\frac{1}{2}, \frac{3}{2})$	$(2,1)$	$\frac{5}{2}$	1	$\frac{3}{2}$	$\frac{4}{3}$	-154	$-\frac{1}{2\sqrt{5}}$	$\frac{1}{15}$
$(\frac{3}{2}, \frac{3}{2})$	$(2,1)$	$\frac{5}{2}$	$\frac{3}{2}$	2	$\frac{8}{3}$	$+358$	$\frac{\sqrt{7}}{10\sqrt{2}}$	$\frac{7}{75}$
$(\frac{5}{2}, \frac{7}{2})$	$(2,1)$	$\frac{5}{2}$	1	$\frac{7}{2}$	8	$+694$	$-\frac{1}{6\sqrt{14}}$	$\frac{1}{63}$
$(\frac{7}{2}, \frac{7}{2})$	$(2,1)$	$\frac{5}{2}$	$\frac{7}{2}$	2	$\frac{32}{3}$	$+804$	$\frac{1}{4\sqrt{7}}$	$\frac{2}{21}$
$(\frac{5}{2}, \frac{3}{2})$	$(2,1)$	$\frac{5}{2}$	2	$\frac{5}{2}$	4	$+902$	$-\frac{\sqrt{7}}{15\sqrt{2}}$	$\frac{14}{225}$

NOTE.—The sum of the relative intensities $\sum_i R_i = 1.0$ for each $\Delta J = 1$ transition.
[a] Frequency offsets in kilohertz (kHz) relative to 112359.285 and 224714.368 MHz for $J = 1 - 0$ and $J = 2 - 1$, respectively (from the spectroscopic constants in Klapper et al. [2003]).

$$N_{\text{tot}}(C^{17}O) = \frac{5.07 \times 10^{15}(T_{ex} + 0.88)}{\nu(\text{GHz})R_i} \frac{\exp(\frac{E_u}{kT_{ex}})}{\exp(\frac{h\nu}{kT_{ex}}) - 1}$$
$$\times \left[\frac{T_B \Delta v(\text{km/s})}{f(J_\nu(T_{ex}) - J_\nu(T_{bg}))} \right] \text{cm}^{-2}, \qquad (93)$$

where ν is the frequency of the hyperfine transition used. For example, if the $F = (5/2) - (5/2)$ hyperfine was chosen for this calculation, $R_i = 3/9$ (see Table 5) and $\nu = 112359.285 + 0.724$ MHz $= 112.360009$ GHz. Equation (93) then becomes:

$$N_{\text{tot}}(C^{17}OC^{17}O) = 1.36 \times 10^{14}(T_{ex} + 0.88) \frac{\exp\left(\frac{5.39}{T_{ex}}\right)}{\exp\left(\frac{5.39}{T_{ex}}\right) - 1}$$
$$\times \left[\frac{T_B \Delta v(\text{km/s})}{f(J_\nu(T_{ex}) - J_\nu(T_{bg}))} \right] \text{cm}^{-2}. \qquad (94)$$

15.3. N_2H^+

N_2H^+ is a multiple-spin coupling molecule due to the interaction between its spin and the quadrupole moments of the two nitrogen nuclei. For a nice detailed description of the hyperfine levels of the $J = 1 - 0$ transition, see Shirley et al. (2005) and Pagani et al. (2009). Since the outer N nucleus has a much larger coupling strength than the inner N nucleus, the hyperfine structure can be determined by a sequential application of the spin coupling:

$$\vec{F}_1 = \vec{J} + \vec{I}_N, \vec{F} = \vec{F}_1 + \vec{I}_N.$$
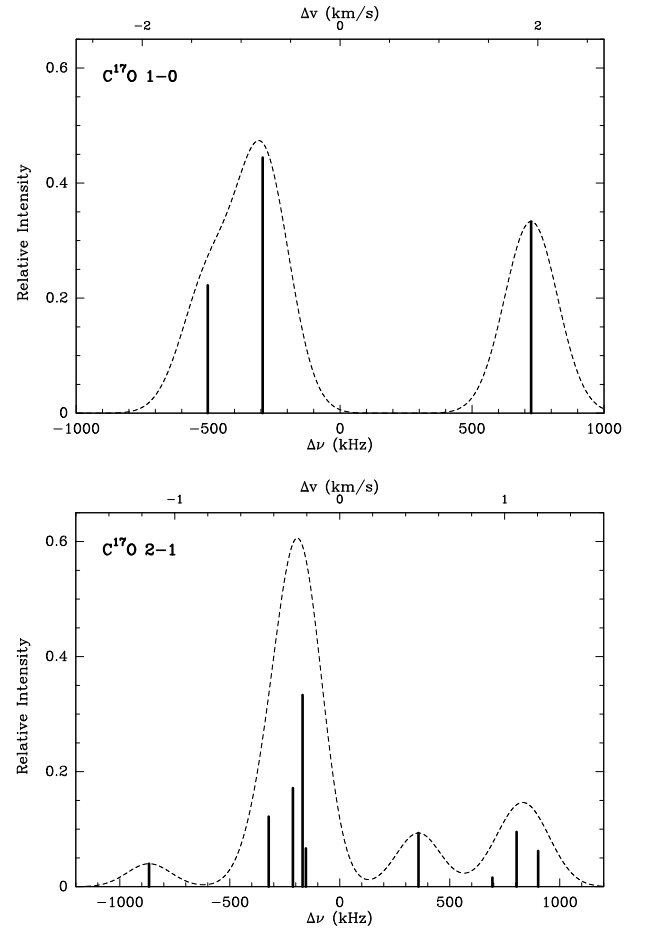
When the coupling from both N nuclei is considered:

FIG. 7.—Synthetic spectra for the $C^{17}O$ $J = 1 - 0$ (*top*) and 2–1 (*bottom*) transitions. Horizontal axes are offset velocity (*top*) and frequency (*bottom*) relative to 112359285.0 and 224714386.0 kHz, respectively. Overlain as a dashed line is a synthetic 100 kHz Gaussian linewidth source spectrum.
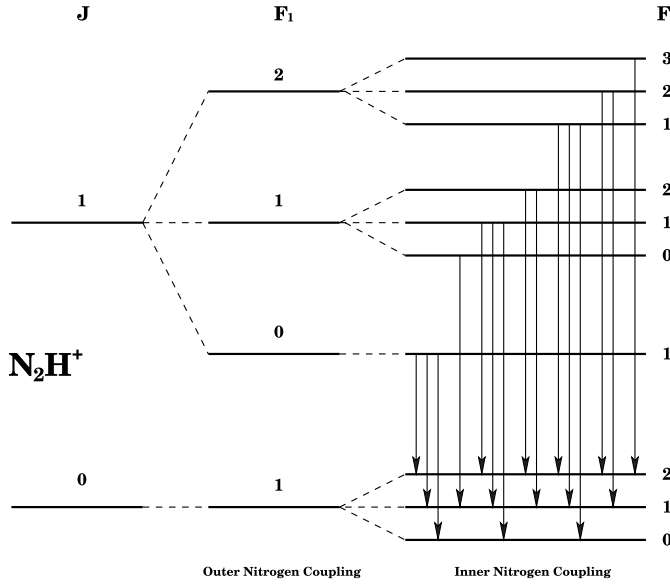
FIG. 8.—Energy level structure for the $J = 1 - 0$ transition of N_2H^+. Note that of the 15 hyperfine split levels, only seven are observed due to the fact that there is no hyperfine splitting of the $J = 0$ level, but it is degenerate in energy. Grouping of the indicated transitions show the seven observed transitions. Transitions are ordered by increasing frequency from left to right.

1. The $J = 0$ level is split into three energy levels.
2. The $J = 1$ level is split into seven energy levels.
3. The $J = 2$ and higher levels are split into nine energy levels.

Since the selection rules for the single-spin coupling case apply, $\Delta F_1 = 0, \pm 1$, $\Delta F = 0, \pm 1$, $0 \nrightarrow 0$, and $\Delta J = \pm 1$, there are 15, 34, and 38 hyperfine transitions for the $J = 1 - 0, J = 2 - 1,$ and $J = 3 - 2$ transitions, respectively. Figure 8 shows the energy level structure for the $J = 1 - 0$ transition.

To illustrate the hyperfine intensity calculation for N_2H^+, we derive the relative intensities for the $J = 1 - 0$ transition. Relative intensities, derived using the formalism presented in § 10 and equation (77), are listed in Tables 6, 7, and 8. Figure 9 shows the synthetic spectrum for the N_2H^+ $J = 1 - 0$ transition.

TABLE 6

OUTER NITROGEN (F_1) HYPERFINE INTENSITIES FOR N_2H^+ $J = 1 - 0$

$F_1' \rightarrow F_1$ [a]	$J' \rightarrow J$ [a]	a	b	c	$\frac{(2F_1'+1)(2F_1+1)}{(2I_N+1)}$	6j	$R_i(F_1, J)$
(0,1)	(1,0)	1	0	1	1	$\frac{1}{3}$	$\frac{1}{9}$
(1,1)	(1,0)	1	1	1	3	$-\frac{1}{3}$	$\frac{1}{3}$
(2,1)	(1,0)	1	1	2	5	$\frac{1}{3}$	$\frac{5}{9}$

[a] $I_N = 1$.

To derive the column density for N_2H^+, we start with the general equation for the total molecular column density (eq. [32]) with:

$$S = \frac{J_u}{2J_u + 1} \text{ (see § 9.1)}$$

$$\mu = 3.37 \text{ Debye} = 3.37 \times 10^{-18} \text{ esu}$$

$$B_0 = 46586.88 \text{ MHz}$$

$$R_i = \text{ (see § 10 or, for } J = 1 - 0, \text{ see Table 8)}$$

$$g_J = 2J_u + 1$$

$$g_K = 1 \text{ (for linear molecules)}$$

$$g_I = 1 \text{ (for linear molecules)}$$

$$Q_{\text{rot}} \simeq \frac{kT}{hB} + \frac{1}{3} \text{ (eq.52)}$$

$$\simeq 0.45(T + 0.74)$$

$$E_u = 4.4716 \text{ K}$$

which leads to:

$$N_{\text{tot}}(N_2H^+) = \frac{3h}{8\pi^3\mu^2} \frac{Q_{\text{rot}}}{J_u R_i} \exp\left(\frac{E_u}{kT_{ex}}\right) \left[\exp\left(\frac{h\nu}{kT_{ex}}\right) - 1\right]^{-1}$$
$$\times \int \tau_\nu d\upsilon. \tag{95}$$

Assuming optically thin emission (eq. [80]), we find that equation (95) becomes:[11]

$$N_{\text{tot}}(N_2H^+) = \frac{6.25 \times 10^{15}}{\nu(\text{GHz})R_i} \frac{\exp(\frac{E_u}{kT_{ex}})}{\exp(\frac{h\nu}{kT_{ex}}) - 1}$$
$$\times \left[\frac{T_B \Delta\upsilon(\text{km/s})}{f(J_\nu(T_{ex}) - J_\nu(T_{bg}))}\right] \text{cm}^{-2}, \tag{96}$$

where ν is the frequency of the hyperfine transition used. For example, if the $F = (2,1)$, $J = (1,0)$ hyperfine was chosen for this calculation, $R_i = 7/27$ (see Table 8) and $\nu = 93.1737767$ GHz. Equation (96) then becomes:

___

[11] Alternatively, one can derive τ using the ratio of two hyperfine transition intensities as described in Appendix D.

TABLE 7
INNER NITROGEN (F) HYPERFINE INTENSITIES FOR N_2H^+ $J = 1 - 0$

$F' \to F$ [a]	$F_1' \to F_1$ [a]	a	b	c	$\frac{(2F'+1)(2F+1)}{(2I_N+1)}$	6j	$R_i(F, F_1)$
(1,0)	(0,1)	1	0	1	1	$\frac{1}{3}$	$\frac{1}{9}$
(1,1)	(0,1)	1	1	1	3	$-\frac{1}{3}$	$\frac{1}{3}$
(1,2)	(0,1)	1	1	2	5	$\frac{1}{3}$	$\frac{5}{9}$
(0,1)	(1,1)	1	1	1	1	$\frac{1}{3}$	$\frac{1}{9}$
(1,0)	(1,1)	1	1	1	1	$-\frac{1}{3}$	$\frac{1}{9}$
(1,1)	(1,1)	1	1	1	3	$\frac{1}{6}$	$\frac{1}{12}$
(1,2)	(1,1)	1	1	2	5	$\frac{1}{6}$	$\frac{5}{36}$
(2,1)	(1,1)	1	1	2	5	$\frac{1}{6}$	$\frac{5}{36}$
(2,2)	(1,1)	1	2	1	$\frac{25}{3}$	$-\frac{1}{2\sqrt{5}}$	$\frac{5}{12}$
(1,0)	(2,1)	1	2	1	1	$\frac{1}{3}$	$\frac{1}{9}$
(1,1)	(2,1)	1	1	2	3	$\frac{1}{6}$	$\frac{1}{12}$
(1,2)	(2,1)	1	1	2	5	$\frac{1}{30}$	$\frac{1}{180}$
(2,1)	(2,1)	1	2	2	5	$-\frac{1}{2\sqrt{5}}$	$\frac{1}{4}$
(2,2)	(2,1)	1	2	2	$\frac{25}{3}$	$-\frac{1}{10}$	$\frac{1}{12}$
(3,2)	(2,1)	1	2	3	$\frac{35}{3}$	$\frac{1}{5}$	$\frac{7}{15}$

[a] $I_N = 1$.

$$N_{\text{tot}}(N_2H^+(3,2;2,1)) = \frac{2.59 \times 10^{14} \exp(\frac{4.47}{T_{ex}})}{\exp(\frac{4.47}{T_{ex}}) - 1}$$
$$\times \left[\frac{T_B \Delta v(\text{km/s})}{f(J_\nu(T_{ex}) - J_\nu(T_{bg}))} \right] \text{cm}^{-2}, \quad (97)$$

TABLE 8
HYPERFINE INTENSITIES FOR N_2H^+ $J = 1 - 0$

$F' \to F$ [a]	$F_1' \to F_1$ [a]	$J' \to J$	$R_i(F_1, J)$ $R_i(F, F_1)$	$\Delta\nu$ (kHz) [a]	R_j(obs) [b]
(0,1)	(1,1)	(1,0)	$\frac{1}{27}$	−2155.7	$\frac{1}{27}$
(2,2)	(1,1)	(1,0)	$\frac{5}{36}$	−1859.9	$\frac{5}{27}$
(2,1)	(1,1)	(1,0)	$\frac{5}{108}$		
(1,2)	(1,1)	(1,0)	$\frac{5}{108}$	−1723.4	$\frac{1}{9}$
(1,1)	(1,1)	(1,0)	$\frac{1}{36}$		
(1,0)	(1,1)	(1,0)	$\frac{1}{27}$		
(2,1)	(2,1)	(1,0)	$\frac{5}{36}$	−297.1	$\frac{5}{27}$
(2,2)	(2,1)	(1,0)	$\frac{5}{108}$		
(3,2)	(2,1)	(1,0)	$\frac{7}{27}$	+0.0	$\frac{7}{27}$
(1,1)	(2,1)	(1,0)	$\frac{5}{108}$	+189.9	$\frac{1}{9}$
(1,2)	(2,1)	(1,0)	$\frac{1}{324}$		
(1,0)	(2,1)	(1,0)	$\frac{5}{81}$		
(1,2)	(0,1)	(1,0)	$\frac{5}{81}$	+2488.3	$\frac{1}{9}$
(1,1)	(0,1)	(1,0)	$\frac{1}{27}$		
(1,0)	(0,1)	(1,0)	$\frac{1}{81}$		

NOTE.—The sum of the relative intensities $\sum_i R_i = 1.0$.
[a] Frequency offset in kilohertz (kHz) relative to 93173.7767 MHz (Caselli et al. 1995).
[b] Since the $J = 0$ level has no hyperfine splitting, only the sum of all transitions into the $J = 0$ is observed.
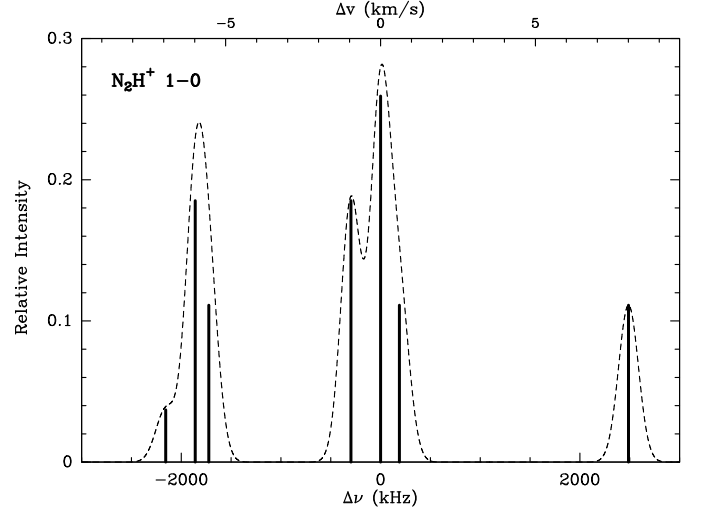
FIG. 9.—Synthetic spectra for the N_2H^+ $J = 1 - 0$ transition. Horizontal axes are offset velocity (*top*) and frequency (*bottom*) relative to 93173.7767 MHz. Overlain as a dashed line is a synthetic 100 kHz ($\Delta v = 0.3218$ km s^{-1}) Gaussian linewidth source spectrum.

where the transition designation is in the $(F', F_1' : F, F_1)$ format. Note that this transition is blended with the nearby $F' = 1$ and 2 $(F_1', F_1) = (2, 1)$ hyperfine transitions under many molecular cloud physical conditions.

15.4. NH_3

Ammonia (NH_3) is a symmetric top molecule with three opposing identical H (spin = 1/2) nuclei. Quantum mechanical tunneling of the N nucleus through the potential energy plane formed by the H nuclei leads to inversion splitting of each NH_3 energy level. On top of this inversion splitting, the energy levels are split due to two hyperfine interactions:

J–I_N: Coupling between the quadrupole moment of the N nucleus ($I_N = 1$) and the electric field of the H atoms, which splits each energy level into three hyperfine states. For this interaction, the angular momentum vectors are defined as follows: $\vec{F}_1 = \vec{J} + \vec{I}_N$.

F_1–I_H: Coupling between the magnetic dipole of the three H nuclei [$I_H = 1/2$ for $K \neq 0$ or $3n$ (para), $I_H = 3/2$ for $K = 3n$ (ortho)] with the weak current generated by the rotation of the molecule. For this interaction, the angular momentum vectors are defined as follows: $\vec{F} = \vec{F}_1 + \vec{I}_H$.

Weaker N–H spin–spin and H–H spin–spin interactions also exist, but only represent small perturbations of the existing hyperfine energy levels.

Figure 10 shows all NH_3 energy levels below 1600 K, while Table 9 lists the level energies for $J \leq 6$. Figure 11 shows the rotational energy level diagram for the first four J-levels of NH_3, while Figure 12 shows the inversion and hyperfine level structure for the (1,1) and (2,2) transitions.

FIG. 10.—Rotational energy level diagram for NH_3. All levels with energy <1600 K are shown.
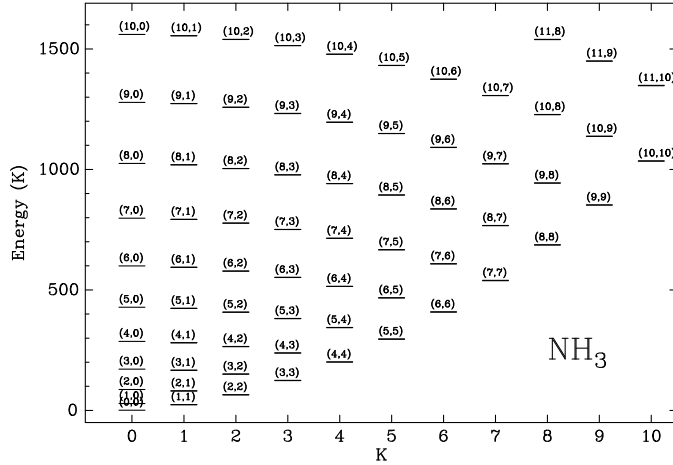
We can calculate the relative hyperfine intensities (R_i) for the (1,1), (2,2), (3,3), and (4,4) transitions using the formalism derived in § 10. Using the formalism presented in § 10 we can derive the relevant R_i for the quadrupole hyperfine [$R_i(F_1, J)$, $I_N = 1$; Tables 11, 12, 13, and 14] and magnetic hyperfine [$R_i(F, F_1)$, $I_H = 1/2$ (para, $K \neq 0$ or $3n$) or $3/2$ (ortho,

TABLE 9
NH_3 LEVEL ENERGIES

Level	Energy (K)	Level	Energy (K)
(0,0,a)	1.14	…	…
(1,1,s)	23.21	(1,1,a)	24.35
(1,0,s)	28.64	…	…
(2,2,s)	64.20	(2,2,a)	65.34
(2,1,s)	80.47	(2,1,a)	81.58
(2,0,a)	86.99	…	…
(3,3,s)	122.97	(3,3,a)	124.11
(3,2,s)	150.06	(3,2,a)	151.16
(3,1,s)	166.29	(3,1,a)	167.36
(3,0,s)	171.70	…	…
(4,4,s)	199.51	(4,4,a)	200.66
(4,3,s)	237.40	(4,3,a)	238.48
(4,2,s)	264.41	(4,2,a)	265.45
(4,1,s)	280.58	(4,1,a)	281.60
(4,0,a)	286.98	…	…
(5,5,s)	293.82	(5,5,a)	295.00
(5,4,s)	342.49	(5,4,a)	343.58
(5,3,s)	380.23	(5,3,a)	381.25
(5,2,s)	407.12	(5,2,s)	408.10
(5,1,s)	423.23	(5,1,a)	424.18
(5,0,s)	428.60	…	…
(6,6,s)	405.91	(6,6,a)	407.12
(6,3,s)	551.30	(6,3,a)	552.25
(6,0,a)	600.30	…	…

NOTES.—Listed in level energy order per J and inversion-paired as appropriate. See Poynter & Kakar (1975) for lower-state energy calculations.

$K = 3n$); Tables 15, 16, 17, and 18] coupling cases. The resultant total hyperfine intensities are derived by multiplying the magnetic hyperfine intensities [$R_i(F, F_1)$] by the associated quadrupole hyperfine intensities [$R_i(F_1, J)$]. Tables 19 and 20 show the results of this calculation for the NH_3 (1,1) and (2,2) transitions, respectively. Figure 13 shows the synthetic spectra for the NH_3 (1,1) and (2,2) transitions.

For illustration, we can derive the column density equation for a para-NH_3 ($K \neq$ or $3n$) inversion ($\Delta K = 0$) transition. For para-NH_3 inversion transitions:

$$S = \frac{K^2}{J_u(J_u + 1)}$$

$$\mu = 1.468 \text{ Debye} = 1.468 \times 10^{-18} \text{ esu}$$

$$R_i = (\text{see § 10 or, for } (1,1) \text{ and } (2,2),$$
$$\text{see Tables 19 and 20})$$

$$g_J = 2J_u + 1$$

$$g_K = 2 \quad \text{for } K \neq 0$$

$$g_I = \frac{2}{8} \quad \text{for } K \neq 3n$$

Doing the calculation in two stages, we can first derive the following equation for the molecular column density in NH_3 as derived from a measurement of a (J, K) inversion ($\Delta J = 0$, $\Delta K = 0$) transition assuming optically thin emission (see Rosolowsky et al. [2008] for the methodology to fit hyperfine transitions in the optically thick limit) using equation (80):

$$N_{tot}(NH_3) = \frac{3h}{8\pi^3\mu^2 R_i} \frac{J_u(J_u + 1)}{K^2} \frac{Q_{rot}}{g_J g_K g_I} \frac{\exp(\frac{E_u}{kT_{ex}})}{\exp(\frac{h\nu}{kT_{ex}}) - 1}$$
$$\times \left[\frac{\int T_R dv}{f(J_\nu(T_{ex}) - J_\nu(T_{bg}))} \right]. \tag{98}$$

Further assuming that we are measuring para-NH_3 ($K \neq$ or $3n$), equation (98) becomes:

$$N_{tot}(NH_3) \simeq \frac{7.44 \times 10^{12} J_u(J_u + 1) Q_{rot}}{R_i K^2 (2J_u + 1)} \frac{\exp(\frac{E_u}{kT_{ex}})}{\exp(\frac{h\nu}{kT_{ex}}) - 1}$$
$$\times \left[\frac{\int T_R dv(\text{km/s})}{f(J_\nu(T_{ex}) - J_\nu(T_{bg}))} \right] \text{cm}^{-2}. \tag{99}$$

15.5. H_2CO

Formaldehyde (H_2CO) is a slightly asymmetric rotor molecule with $\kappa \simeq -0.961$ (eq. [45]), which means that H_2CO is nearly a prolate symmetric rotor. The slight asymmetry in H_2CO results in limiting prolate (quantum number K_{-1}) and oblate (quantum number K_{+1}) symmetric rotor energy levels

TABLE 10
F_1–I_H Hyperfine Frequencies and Intensities for H_2CO $J = 1, 2,$ and 3 K-Doublet Transitions

$F' \to F$[a]	$J' \to J$[a]	Δ_{HF}[b] (kHz)	a	b	c	$\frac{(2F'_1+1)(2F_1+1)}{(2I_H+1)}$	6j	$R_i(F_1, J)$
(1,0)	(1,1)	−18.53	1	1	1	1	$-\frac{1}{3}$	$\frac{1}{9}$
(0,1)	(1,1)	−1.34	1	1	1	1	$-\frac{1}{3}$	$\frac{1}{9}$
(2,2)	(1,1)	−0.35	1	2	1	$\frac{25}{3}$	$-\frac{1}{2\sqrt{5}}$	$\frac{5}{12}$
(2,1)	(1,1)	+4.05	1	1	2	5	$\frac{1}{6}$	$\frac{5}{36}$
(1,2)	(1,1)	+6.48	1	1	2	5	$\frac{1}{6}$	$\frac{5}{36}$
(1,1)	(1,1)	+11.08	1	1	1	3	$\frac{1}{6}$	$\frac{1}{12}$
(1,1)	(2,2)	−20.73	1	1	2	3	$\frac{1}{2\sqrt{5}}$	$\frac{3}{20}$
(1,2)	(2,2)	−8.5	1	2	2	5	$-\frac{1}{10}$	$\frac{1}{20}$
(2,1)	(2,2)	−0.71	1	2	2	5	$-\frac{1}{10}$	$\frac{1}{20}$
(3,3)	(2,2)	+0.71	1	3	2	$\frac{49}{3}$	$-\frac{2\sqrt{2}}{3\sqrt{35}}$	$\frac{392}{945}$
(3,2)	(2,2)	+1.42	1	2	3	$\frac{35}{3}$	$\frac{1}{15}$	$\frac{7}{135}$
(2,3)	(2,2)	+9.76	1	2	3	$\frac{35}{3}$	$\frac{1}{15}$	$\frac{7}{135}$
(2,2)	(2,2)	+10.12	1	2	2	$\frac{25}{3}$	$\frac{1}{6}$	$\frac{25}{108}$
(2,3)	(3,3)	…	1	3	3	$\frac{35}{3}$	$-\frac{1}{21}$	$\frac{5}{189}$
(4,3)	(3,3)	…	1	3	4	21	$\frac{1}{28}$	$\frac{3}{112}$
(4,4)	(3,3)	+0.00	1	4	3	27	$-\frac{\sqrt{5}}{4\sqrt{21}}$	$\frac{45}{112}$
(3,3)	(3,3)	−10.4	1	3	3	$\frac{49}{3}$	$\frac{11}{84}$	$\frac{121}{432}$
(2,2)	(3,3)	+23.0	1	2	3	$\frac{25}{3}$	$\frac{-2\sqrt{2}}{3\sqrt{35}}$	$\frac{40}{189}$
(3,4)	(3,3)	…	1	3	4	21	$\frac{1}{28}$	$\frac{3}{112}$
(3,2)	(3,3)	…	1	3	3	$\frac{35}{3}$	$-\frac{1}{21}$	$\frac{5}{189}$

[a] $I_H = 1$ (ortho-H_2CO).

[b] Frequency offset in kilohertz (kHz) relative to 4829.6596 MHz for $1_{10} - 1_{11}$, 14488.65 MHz for $2_{11} - 2_{12}$, and 28974.85 MHz for $3_{12} - 3_{13}$.
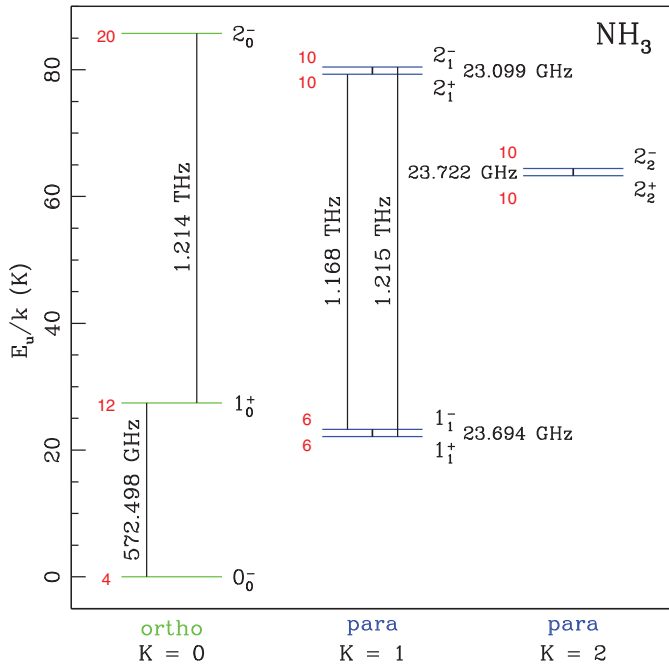

FIG. 11.—Ammonia energy levels below 100 K. The notation $J_K^\pm$ is used where $\pm$ refers to the symmetry of the energy level. Allowed electric dipole transitions are indicated with frequencies of the transitions. The total statistical weight of each energy level is indicated in red to the left of each energy level.

that are closely spaced in energy, a feature commonly referred to as "K-doublet splitting." Figure 14 shows the energy level diagram for H_2CO including all energy levels $E \leq 300$ K. In addition to the asymmetric rotor energy level structure, H_2CO possesses spin–rotation and spin–spin hyperfine energy level structure. Magnetic dipole interaction between the H nuclei ($I_H = 0/1$ for para-/ortho-H_2CO) and rotational motion of the molecule result in spin–rotation hyperfine energy level splitting. Since the two H nuclei have equal coupling, the two H nuclei spins couple with each other first and the hyperfine coupling scheme is $\vec{I}_H = \vec{I}_1 + \vec{I}_2$ and $\vec{F} = \vec{J} + \vec{I}_H$. Since the interchange of the two ^{1}H atoms ($I_1 = I_2 = 1/2$) obey Fermi–Dirac statistics (total wave function is antisymmetric to this interchange) and alternating K_a ladders in H_2CO have a different rotational wavefunction symmetry, only ortho-H_2CO levels ($I_H = 1$) with $K_a =$ odd integers have hyperfine splitting. For the ortho-H_2CO $1_{10} - 1_{11}$ transition, the frequency offsets of these hyperfine transitions are $\Delta\nu \leq 18.5$ kHz. The weaker spin–spin interactions between the nuclei are generally not considered.

Table 10 lists the frequencies and relative intensities for the spin–rotation hyperfine transitions of the H_2CO $1_{10} - 1_{11}$, $2_{11} - 2_{12}$, and $3_{12} - 3_{13}$ transitions. Figure 15 shows the synthetic spectra for the H_2CO $1_{10} - 1_{11}$, $2_{11} - 2_{12}$, and $3_{12} - 3_{13}$ transitions. Note that the hyperfine intensities are exactly equal to those calculated for the spin-rotation hyperfine components of NH_3 (see Appendix F).
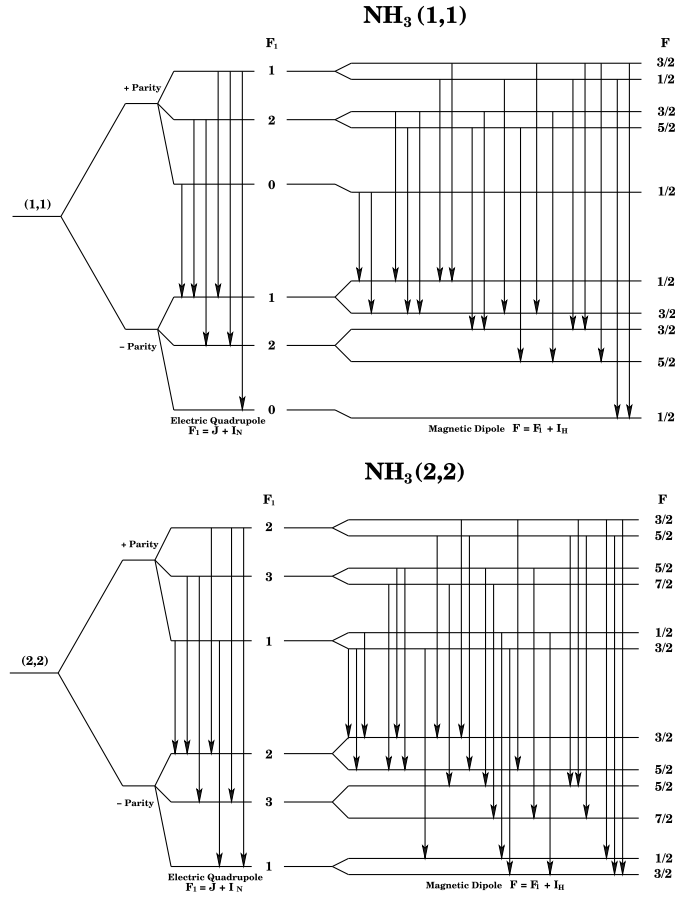
NH₃ (1,1)

NH₃ (2,2)

FIG. 12.—Inversion and hyperfine energy level structure for the (1,1) (*top*) and (2,2) (*bottom*) transitions of NH₃. Note that the 18 (1,1) and 24 (2,2) allowed transitions are marked with arrows ordered by increasing frequency from left to right. Adapted from Ho & Townes (1983).

For illustration we can derive the column density equation for a ortho-H₂CO (K_{-1} odd) K-doublet ($\Delta K_{-1} = 0$) transition. For ortho-H₂CO transitions:

$$S = \frac{K^2}{J_u(J_u + 1)}$$

$$\mu = 2.331 \text{ Debye} = 2.331 \times 10^{-18} \text{ esu}$$

$$R_i = (\text{see § 10 or, for } 1_{10} - 1_{11}, 2_{11} - 2_{12},$$
$$\text{or } 3_{12} - 3_{13} \text{ see Table 10})$$

$$g_J = 2J_u + 1$$

$g_K = 2$ for $K \neq 0$ (using the slightly-asymmetricrotor

approximation),

$$g_I = \frac{3}{4}$$ for K_{-1} odd

We can derive the following equation for the molecular column density in H₂CO as derived from a measurement of an
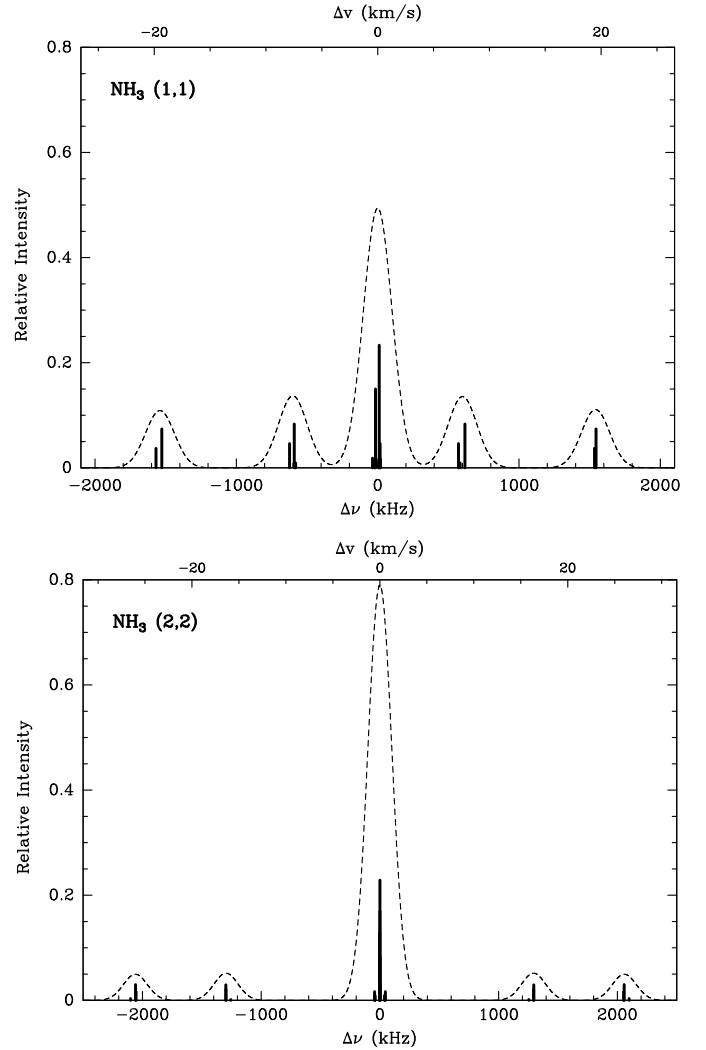
FIG. 13.—Synthetic spectra for the NH₃ (1,1) (*top*) and (2,2) (*bottom*) transitions. Horizontal axes are offset velocity (*top*) and frequency (*bottom*) relative to 23694.495487 and 23722.633335 MHz, respectively. Overlain as a dashed line is a synthetic 100 kHz ($\Delta v = 1.265$ and 1.264 km s^{-1}, respectively) Gaussian linewidth source spectrum.

ortho-H₂CO (K_{-1} odd) K-doublet transition assuming optically thin emission using equation (80):

$$N_{\text{tot}}(\text{H}_2\text{CO}) = \frac{3h}{8\pi^3\mu^2 R_i} \frac{J_u(J_u + 1)}{K^2} \frac{Q_{\text{rot}}}{g_J g_K g_I} \frac{\exp(\frac{E_u}{kT_{ex}})}{\exp(\frac{h\nu}{kT_{ex}}) - 1}$$

$$\times \left[\frac{\int T_R dv}{f(J_\nu(T_{ex}) - J_\nu(T_{bg}))} \right]$$

$$\simeq \frac{9.83 \times 10^{11} J_u(J_u + 1) Q_{\text{rot}}}{R_i K^2 (2J_u + 1)} \frac{\exp(\frac{E_u}{kT_{ex}})}{\exp(\frac{h\nu}{kT_{ex}}) - 1}$$

$$\times \left[\frac{\int T_R dv(\text{km/s})}{f(J_\nu(T_{ex}) - J_\nu(T_{bg}))} \right] \text{cm}^{-2}. \qquad (100)$$
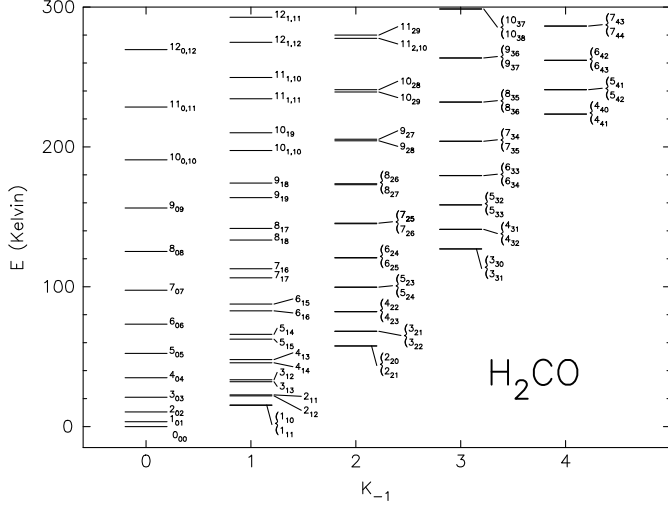
FIG. 14.—Rotational energy level diagram for H_2CO including all energy levels with $E \leq 300$ K.

Note that the K-doublet transitions of H_2CO are rather unusual in that, due to an unusual collisional excitation effect, these transitions are often measured in *absorption* against the cosmic microwave background radiation. For $n(H_2) \lesssim 10^{5.5}$ cm^{-3}, a collisional selection effect overpopulates the lower energy states of the $1_{10} - 1_{11}$ through $5_{14} - 5_{15}$ transitions (Evans et al. 1975; Garrison et al. 1975). This overpopulation of the lower energy states results in a "cooling" of the $J \leq 5$ K-doublets to an excitation temperature that is lower than that of the cosmic microwave background. This causes the $J \leq 5$ K-doublet transitions to appear in absorption. For volume densities $n(H_2) \gtrsim 10^{5.5}$ cm^{-3} and $T_K \simeq 40$ K, this collisional pump is quenched. For these higher-volume densities the $J \leq 5$ K-doublets are driven into emission over a wide range of kinetic temperatures and abundances (see Fig. 1 in Mangum et al. [2008]).

16. SUMMARY

The most general form of the molecular spectral line column density is given by equation (32):

$$N_{tot} = \frac{3h}{8\pi^3 |\mu_{lu}|^2} \frac{Q_{rot}}{g_u} \exp\left(\frac{E_u}{kT_{ex}}\right)\left[\exp\left(\frac{h\nu}{kT_{ex}}\right) - 1\right]^{-1}$$
$$\times \int \tau_\nu dv. \tag{101}$$

For absorption line measurements one should use the velocity integrated opacity directly in equation (32). For emission lines, the velocity integrated opacity is usually converted to an integrated intensity. In the optically thin limit, the column density becomes (eq. [80]):
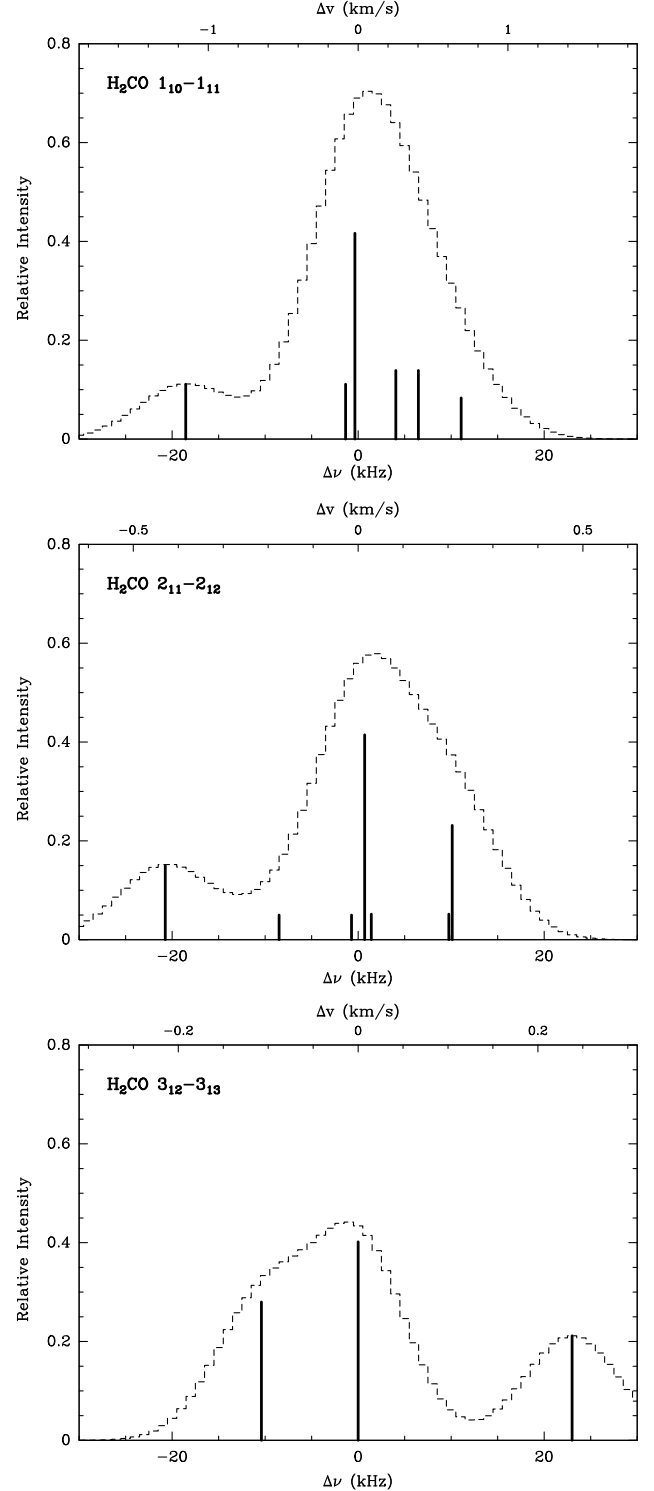
FIG. 15.—Synthetic spectra for the H_2CO $1_{10} - 1_{11}, 2_{11} - 2_{12}$, and $3_{12} - 3_{13}$ transitions. Horizontal axes are offset velocity (top) and frequency (bottom) relative to 4829.6596 MHz for $1_{10} - 1_{11}$, 14488.650 MHz for $2_{11} - 2_{12}$, and 28974.85 MHz for $3_{12} - 3_{13}$, respectively. For the $3_{12} - 3_{13}$ transition only the $\Delta F = 0$ hyperfine transitions are shown. Overlain as a dashed line is a synthetic 10 kHz ($\Delta v = 0.621, 0.207$, and 0.103 km s^{-1}, respectively) Gaussian linewidth source spectrum.

$$N_{\text{tot}}^{\text{thin}} = \left(\frac{3h}{8\pi^3 S\mu^2 R_i}\right)\left(\frac{Q_{\text{rot}}}{g_J g_K g_I}\right)\frac{\exp(\frac{E_u}{kT_{ex}})}{\exp(\frac{h\nu}{kT_{ex}}) - 1}$$
$$\times \frac{1}{(J_\nu(T_{ex}) - J_\nu(T_{bg}))}\int\frac{T_R dv}{f}. \tag{102}$$

The optically thick column density is related to the optically thin column density by equation (86):

$$N_{\text{tot}} = N_{\text{tot}}^{\text{thin}}\frac{\tau}{1 - \exp(-\tau)}. \tag{103}$$

In this tutorial, we have carefully derived the terms in equations (32), (80), and (86). Note, though, that these equations assume all energy levels are characterized by the same excitation temperature (the "CTEX LTE approximation"; see § 12). We have also explored the limits of the CTEX approximation (§ 12). Non-LTE determinations of the column density require a coupled radiative transfer and statistical equilibrium calculation and can be performed with publically available tools.

APPENDIX A.

LINE PROFILE FUNCTIONS

For a Gaussian profile, the function $\phi(\nu)$ is given by

$$\phi(\nu) = \frac{1}{\sqrt{2\pi}\sigma}\exp\left[-\frac{(\nu - \nu_0)^2}{2\sigma^2}\right], \tag{A1}$$

where ν_0 and ν are the central and offset frequencies of the line profile for a particle with mass M and velocity v,

$$2\sigma^2 = \frac{\nu_0^2}{c^2}\left(\frac{2kT_k}{M} + v^2\right), \tag{A2}$$

and

$$\int\phi(\nu)d\nu = 1. \tag{A3}$$

The Gaussian profile has a FWHM given by (in both frequency and velocity):

$$\Delta\nu_D = \frac{2\nu_0}{c}\left[\ln 2\left(\frac{2kT_k}{M} + v^2\right)\right]^2 \tag{A4}$$

$$\Delta v_D = 2\left[\ln 2\left(\frac{2kT_k}{M} + v^2\right)\right]^2, \tag{A5}$$

and a peak value given by:

$$\phi(\nu)_{\text{peak}} = \frac{2\sqrt{\ln 2}}{\sqrt{\pi}\Delta\nu_D}$$
$$= \frac{2\sqrt{\ln 2}c}{\sqrt{\pi}\nu_0\Delta v_D}. \tag{A6}$$

If one uses peak values instead of integrating over a Gaussian profile to derive column densities, one must make the following correction:

$$(N_{\text{tot}})_{\text{Gauss}} = 2\sqrt{\frac{\ln 2}{\pi}}(N_{\text{tot}})_{\text{peak}}. \tag{A7}$$

APPENDIX B.

INTEGRATED FLUXES VERSUS BRIGHTNESS TEMPERATURES

All calculations in this document assume the use of integrated brightness temperatures ($\int T_B\Delta v$). If one uses integrated fluxes ($\int S_\nu\Delta v$), the total molecular column density assuming optically thin emission (eq. [82]) is modified by using the relationship between flux density and brightness temperature:

$$S_\nu = \frac{2kT_B\nu^2}{c^2}\Omega_s, \tag{B1}$$

and becomes

$$N_{\text{tot}} = \left(\frac{D}{2R_s}\right)^2\frac{3c^2}{16\pi^3 S\mu^2\nu^3}\left(\frac{Q_{\text{rot}}}{g_J g_K g_{\text{nuclear}}}\right)\exp\left(\frac{E_u}{kT}\right)\int S_\nu\Delta v$$
$$= \frac{3c^2}{16\pi^3\Omega_s S\mu^2\nu^3}\left(\frac{Q_{\text{rot}}}{g_J g_K g_{\text{nuclear}}}\right)\exp\left(\frac{E_u}{kT}\right)\int S_\nu\Delta v. \tag{B2}$$

APPENDIX C.

INTEGRATED INTENSITY UNCERTAINTY

For cases where you do not have a calculation from a fit to the integrated intensity of a spectral line, one can use the following estimate given a measurement of the baseline rms and line profile properties.

$$\int T dv = \Delta v_c \sum_{n=1}^{N} T_n,$$
$$\equiv I \qquad (C1)$$

where Δv_c is the spectral velocity channel width, T_n is a spectral channel value, and the line spans N channels. The statistical uncertainty of the integrated line intensity is given by:

$$\sigma_I^2 = \sum_{n=1}^{N} \sigma_{T_n}^2 \left[\frac{\partial I}{\partial T}\right]^2 + \sigma_{\Delta v_c}^2 \left[\frac{\partial I}{\partial (\Delta v_c)}\right]^2$$
$$= \sum_{n=1}^{N} \sigma_{T_n}^2 (\Delta v_c)^2$$
$$= N \sigma_T^2 (\Delta v_c)^2, \qquad (C2)$$

where we have used the fact that we know the velocity channel width ($\sigma_{\Delta v_c} = 0$) and assuming that all of the channel noise values are equal. We can then write equation (C2) as follows:

$$\sigma_I = \sqrt{N} \sigma_T \Delta v_c$$
$$= \sigma_T \sqrt{\Delta v_{\text{line}} \Delta v_c}, \qquad (C3)$$

where we have used the fact that the spectral line width $\Delta v_{\text{line}} = N \Delta v_c$ to get the last expression for σ_I.

APPENDIX D.

HYPERFINE RATIOS AND OPTICAL DEPTH

For molecules with measurable hyperfine splitting one can derive an estimate of the optical depth in a given transition. Starting with the form of the radiative transfer equation which involves the observable *source radiation temperature* T_R (eq. [27]), we can write the ratio of two hyperfine transitions as follows:

$$\frac{T_R(m)}{T_R(s)} = \frac{f_m[J_\nu(T_{ex,m}) - J_\nu(T_{bg})][1 - \exp(-\tau_{\nu,m})]}{f_s[J_\nu(T_{ex,s}) - J_\nu(T_{bg})][1 - \exp(-\tau_{\nu,s})]}, \quad (D1)$$

where m and s refer to the main and satellite hyperfine components of a given rotational transition.[12] If we further assume that the hyperfine levels are in LTE $[J_\nu(T_{ex,m}) = J_\nu(T_{ex,s})]$[13] and that the two hyperfine components emit over the same volume of gas ($f_m = f_s$), Equation (D1) becomes:

$$\frac{T_R(m)}{T_R(s)} = \frac{1 - \exp(-\tau_{\nu,m})}{1 - \exp(-\tau_{\nu,s})}. \qquad (D2)$$

In equilibrium the optical depths of the hyperfine transitions within a given rotational transition should be proportional to their relative intensities:

$$\frac{\tau_{\nu,s}}{\tau_{\nu,m}} = \frac{R_{i,s}}{R_{i,m}}. \qquad (D3)$$

Inserting equation (D3) into equation (D2) results in a simple equation which allows for the calculation of the optical depth of a hyperfine transition (and, therefore, the rotational transition under study) using just the measured intensities of two of its component hyperfine transitions:

$$\frac{T_R(m)}{T_R(s)} = \frac{1 - \exp(-\tau_{\nu,m})}{1 - \exp(-\frac{R_{i,s}}{R_{i,m}} \tau_{\nu,m})}. \qquad (D4)$$

Taking the strongest and second-strongest transitions of the NH_3 (1,1) transition, from Table 11 we find that:

$$\frac{T_R(m)}{T_R(s)} (NH_3(1,1)) = \frac{1 - \exp(-\tau_{\nu,m})}{1 - \exp(-\frac{5}{18}\tau_{\nu,m})}. \qquad (D5)$$

---

[12] Equivalently, one can use molecular isotopologues with the additional assumptions that one knows the isotopic ratio and there is no fractionation between that atomic ratio and the molecular ratio.

[13] But note that anomalous hyperfine excitation has been observed in some molecules (see Section 10), notably the HCN $J = 1 - 0$ transition (Loughnane et al. 2012). This would invalidate the equal-excitation temperature assumption.

APPENDIX E.

EXCITATION AND KINETIC TEMPERATURE

This section is drawn from Appendix A of Mangum et al. (1992). If the metastable ($J = K$; $A_{ij} < 10^{-7}$ s^{-1}) states in NH$_3$ are coupled only through collisions and the populations in the upper nonmetastable ($J \neq K$; $A_{ij} \sim 0.01$ s^{-1}) states in each K-ladder can be neglected, the populations in the metastable states are related through the Boltzmann equation. In molecular clouds, though, $\Delta K = 1$ collisions across K-ladders will deplete metastable states in favor of their next lower J metastable states. Therefore, for example, collisional de-excitation of the (2,2) transition will result in an increase in the population of the (2,1) state, followed by quick radiative relaxation of the (2,1) state into the (1,1) state. This implies that an excitation temperature, $T_{ex}(J', K'; J, K)$ relating the populations in the (J', K') and (J, K) states, $n(J', K')$ and $n(J, K)$, may be derived. From the Boltzmann equation

$$\frac{n(J', K')}{n(J, K)} = \frac{g(J', K')}{g(J, K)} \exp\left[-\frac{\Delta E(J', K'; J, K)}{T_{ex}(J', K'; J, K)}\right], \quad \text{(E1)}$$

and the ratio of level (J', K') and (J, K) column densities [assuming $h\nu \ll kT_{ex}(J', K'; J, K)$] for the (J, K) and (J', K') transitions

$$\frac{N(J', K')}{N(J, K)} = \frac{J'(J' + 1)K^2\tau(J', K')\Delta v(J', K')}{J(J + 1)(K')^2\tau(J, K)\Delta v(J, K)}, \quad \text{(E2)}$$

and the fact that in a homogeneous molecular cloud

$$\frac{n(J', K')}{n(J, K)} = \frac{N(J', K')}{N(J, K)}, \quad \text{(E3)}$$

we find that

$$\frac{g(J', K')}{g(J, K)} \exp\left[-\frac{\Delta E(J', K'; J, K)}{T_{ex}(J', K'; J, K)}\right]$$
$$= \frac{J'(J' + 1)K^2\tau(J', K')\Delta v(J', K')}{J(J + 1)(K')^2\tau(J, K)\Delta v(J, K)}. \quad \text{(E4)}$$

Using

$$\tau(J, K) = \left[\sum^{F, F'} R_{F, F'} \bigg/ \sum^{F, F'} R_m\right]\tau(J, K, m), \quad \text{(E5)}$$

where R is the relative intensity for a quadrupole (F, F_1) or main (m) hyperfine component, and

$$I_{JK} \equiv \left[\sum^{F, F'} R_{F, F'} \bigg/ \sum^{F, F'} R_m\right],$$

$$= \frac{1.0}{\frac{5}{12} + \frac{1}{12}},$$

$$= 2.000 \text{ for the } (1, 1) \text{ transition (see Tables 11 or 19)},$$

$$= \frac{1.0}{\frac{56}{135} + \frac{25}{108} + \frac{3}{20}},$$

$$= 1.256 \text{ for the } (2, K) \text{ transitions (see Tables 12 or 20)},$$

$$= \frac{54}{43},$$

$$= \frac{1.0}{\frac{45}{112} + \frac{121}{432} + \frac{40}{189}},$$

$$= \frac{216}{193},$$

$$= 1.119 \text{ for the } (3, K) \text{ transitions (see Table 13)},$$

$$= \frac{1.0}{\frac{968}{2475} + \frac{361}{1200} + \frac{35}{144}},$$

$$= \frac{2200}{2057},$$

$$= 1.070 \text{ for the } (4, K) \text{ transitions (see Table 14)},$$

for the (1,1) and (2,2) transitions, we can relate the total optical depth $\tau(J, K)$ to the optical depth in the main hyperfine component $\tau(J, K, m)$, noting that for NH$_3$ $g(J, K) = 2J_u + 1$, and solving equation (E4) for $T_{ex}(J', K'; J, K)$ we find that

$$T_{ex}(J', K'; J, K) = -\Delta E(J', K'; J, K)$$
$$\times \left\{\ln\left[\frac{(2J+1)J'(J'+1)K^2 I_{J'K'}\tau(J', K', m)\Delta v(J', K')}{(2J'+1)J(J+1)(K')^2 I_{JK}\tau(J, K, m)\Delta v(J, K)}\right]\right\}^{-1}. \quad \text{(E6)}$$

Using

$$\frac{T_B(J, K, m)}{T_B(J', K', m)} = \frac{1 - \exp[-\tau(J, K, m)]}{1 - \exp[-\tau(J', K', m)]}, \quad \text{(E7)}$$

which assumes equal excitation temperatures and beam filling factors in the (J, K) and (J', K') transitions. Solving equation (E7) for $\tau(J', K', m)$ yields

$$\tau(J', K', m) = -\ln\left[1 - \frac{T_B(J', K', m)}{T_B(J, K, m)}\right.$$
$$\left. \times \{1 - \exp[-\tau(J, K, m)]\}\right]. \qquad (E8)$$

Substituting equation (E8) into equation (E6):

$$T_{ex}(J', K'; J, K) = -\Delta E(J', K'; J, K)$$
$$\times \left\{ \ln\left[\frac{(2J+1)J'(J'+1)K^2 I_{J'K'}\Delta v(J', K')}{(2J'+1)J(J+1)(K')^2 I_{JK}\tau(J, K, m)\Delta v(J, K)}\right.\right.$$
$$\left.\left.\times \ln\left(1 - \frac{T_B(J', K', m)}{T_B(J, K, m)}\{1 - \exp[-\tau(J, K, m)]\}\right)\right]\right\}^{-1}. \qquad (E9)$$

For $(J', K') = (2, 2)$ and $(J, K) = (1, 1)$, equation (E9) becomes:

$$T_{ex}(2, 2; 1, 1) = -41.5\left\{\ln\left[-\frac{0.283\Delta v(2, 2)}{\tau(1, 1, m)\Delta v(1, 1)}\right.\right.$$
$$\left.\left.\times \ln\left(1 - \frac{T_B(2, 2, m)}{T_B(1, 1, m)}\{1 - \exp[-\tau(1, 1, m)]\}\right)\right]\right\}^{-1}. \qquad (E10)$$

To derive the gas kinetic temperature from $T_{ex}(2, 2; 1, 1)$, one uses statistical equilibrium (noting that only collisional processes are allowed between the different K-ladders), detailed balance, and the Boltzmann equation to calculate T_K from $T_{ex}(J', K'; J, K)$. Assuming that the populations in the $(1,1)$ and $(2,2)$ transitions are much greater than that in the higher lying levels of para-NH_3 and that the population of the nonmetastable $(2,1)$ level is negligible in comparison to that in the $(1,1)$ level, we can use this "three-level model" of NH_3 to analytically derive an expression relating $T_{ex}(2, 2; 1, 1)$ and T_K

$$1 + \frac{C(2, 2; 2, 1)}{C(2, 2; 1, 1)} = \left\{\frac{g(1, 1)}{g(2, 2)}\exp\left[\frac{\Delta E(2, 2; 1, 1)}{T_{ex}(2, 2; 1, 1)}\right]\right\}$$
$$\times \left\{\frac{g(2, 2)}{g(1, 1)}\exp\left[-\frac{\Delta E(2, 2; 1, 1)}{T_K}\right]\right\}, \qquad (E11)$$

where $C(J', K'; J, K)$ is the collisional excitation rate at temperature T_K between levels (J', K') and (J, K). Equation (E11) can be rewritten as

$$T_{ex}(2, 2; 1, 1)\left\{1 + \left(\frac{T_K}{41.5}\right)\ln\left[1 + \frac{C(2, 2; 2, 1)}{C(2, 2; 1, 1)}\right]\right\} - T_K = 0. \qquad (E12)$$

Solutions of equation (E12) give T_K for a measured $T_{ex}(2, 2; 1, 1)$.

APPENDIX F.

NH_3 FREQUENCY AND RELATIVE INTENSITY CALCULATION TABLES

TABLE 11
$J - I_N$ HYPERFINE INTENSITIES FOR $NH_3(1,1)$

$F_1' \to F_1$ [a]	$J' \to J$ [a]	a	b	c	$\frac{(2F_1'+1)(2F_1+1)}{(2I_N+1)}$	6j	$R_i(F_1, J)$
(0,1)	(1,1)	1	1	1	1	$-\frac{1}{3}$	$\frac{1}{9}$
(2,1)	(1,1)	1	1	2	5	$\frac{1}{6}$	$\frac{5}{36}$
(2,2)	(1,1)	1	2	1	$\frac{25}{3}$	$-\frac{1}{2\sqrt{5}}$	$\frac{5}{12}$
(1,1)	(1,1)	1	1	1	3	$\frac{1}{6}$	$\frac{1}{12}$
(1,2)	(1,1)	1	1	2	5	$\frac{1}{6}$	$\frac{5}{36}$
(1,0)	(1,1)	1	1	1	1	$-\frac{1}{3}$	$\frac{1}{9}$

[a] $I_N = 1$.

TABLE 12
$J - I_N$ HYPERFINE INTENSITIES FOR NH_3 (2, K)

$F_1' \to F_1$ [a]	$J' \to J$ [a]	a	b	c	$\frac{(2F_1'+1)(2F_1+1)}{(2I_N+1)}$	6j	$R_i(F_1, J)$
(1,2)	(2,2)	1	2	2	5	$-\frac{1}{10}$	$\frac{1}{20}$
(3,2)	(2,2)	1	2	3	$\frac{35}{3}$	$\frac{1}{15}$	$\frac{7}{135}$
(3,3)	(2,2)	1	3	2	$\frac{49}{3}$	$-\frac{2\sqrt{2}}{3\sqrt{35}}$	$\frac{56}{135}$
(2,2)	(2,2)	1	2	2	$\frac{25}{3}$	$\frac{1}{6}$	$\frac{25}{108}$
(1,1)	(2,2)	1	1	2	3	$-\frac{1}{2\sqrt{5}}$	$\frac{3}{20}$
(2,3)	(2,2)	1	2	3	$\frac{35}{3}$	$\frac{1}{15}$	$\frac{7}{135}$
(2,1)	(2,2)	1	2	2	5	$-\frac{1}{10}$	$\frac{1}{20}$

[a] $I_N = 1$.

TABLE 13

$J - I_N$ HYPERFINE INTENSITIES FOR NH$_3$ (3,K)

$F'_1 \rightarrow F_1$ [a]	$J' \rightarrow J$ [a]	a	b	c	$\frac{(2F'_1+1)(2F_1+1)}{(2I_N+1)}$	6j	$R_i(F_1, J)$
(2,3)	(3,3)	1	3	3	$\frac{35}{3}$	$-\frac{1}{21}$	$\frac{5}{189}$
(4,3)	(3,3)	1	3	4	21	$\frac{1}{28}$	$\frac{3}{112}$
(4,4)	(3,3)	1	4	3	27	$-\frac{\sqrt{5}}{4\sqrt{21}}$	$\frac{45}{112}$
(3,3)	(3,3)	1	3	3	$\frac{49}{3}$	$\frac{11}{84}$	$\frac{121}{432}$
(2,2)	(3,3)	1	2	3	$\frac{25}{3}$	$-\frac{2\sqrt{2}}{3\sqrt{35}}$	$\frac{40}{189}$
(3,4)	(3,3)	1	3	4	21	$\frac{1}{28}$	$\frac{3}{112}$
(3,2)	(3,3)	1	3	3	$\frac{35}{3}$	$-\frac{1}{21}$	$\frac{5}{189}$

[a] $I_N = 1$.

TABLE 14

$J - I_N$ HYPERFINE INTENSITIES FOR (4, K)

$F'_1 \rightarrow F_1$ [a]	$J' \rightarrow J$ [a]	a	b	c	$\frac{(2F'_1+1)(2F_1+1)}{(2I_N+1)}$	6j	$R_i(F_1, J)$
(3,4)	(4,4)	1	4	4	21	$-\frac{1}{36}$	$\frac{7}{432}$
(5,4)	(4,4)	1	4	5	33	$\frac{1}{45}$	$\frac{11}{675}$
(4,4)	(4,4)	1	4	4	27	$\frac{19}{180}$	$\frac{361}{1200}$
(5,5)	(4,4)	1	5	4	$\frac{121}{3}$	$-\frac{2\sqrt{2}}{5\sqrt{33}}$	$\frac{968}{2475}$
(3,3)	(4,4)	1	3	4	$\frac{49}{3}$	$-\frac{\sqrt{5}}{4\sqrt{21}}$	$\frac{35}{144}$
(4,5)	(4,4)	1	4	5	33	$\frac{1}{45}$	$\frac{11}{675}$
(4,3)	(4,4)	1	4	4	21	$-\frac{1}{36}$	$\frac{7}{432}$

[a] $I_N = 1$.

TABLE 15

$F_1 - I_H$ HYPERFINE FREQUENCIES AND INTENSITIES FOR NH$_3$ (1,1)

$F' \rightarrow F$ [a]	$F'_1 \rightarrow F_1$ [a]	$\Delta\nu_{HF}$ [b] (kHz)	a	b	c	$\frac{(2F'+1)(2F+1)}{(2I_H+1)}$	6j	$R_i(F, F_1)$
$(\frac{1}{2},\frac{1}{2})$	(0,1)	−1568.487	$\frac{1}{2}$	$\frac{1}{2}$	1	2	$\frac{1}{\sqrt{6}}$	$\frac{1}{3}$
$(\frac{1}{2},\frac{3}{2})$	(0,1)	−1526.950	$\frac{1}{2}$	1	$\frac{3}{2}$	4	$-\frac{1}{\sqrt{6}}$	$\frac{2}{3}$
$(\frac{3}{2},\frac{1}{2})$	(2,1)	−623.306	$\frac{1}{2}$	2	$\frac{3}{2}$	4	$\frac{2}{\sqrt{3}}$	$\frac{1}{3}$
$(\frac{5}{2},\frac{3}{2})$	(2,1)	−590.338	$\frac{1}{2}$	2	$\frac{5}{2}$	12	$-\frac{1}{2\sqrt{5}}$	$\frac{3}{5}$
$(\frac{3}{2},\frac{3}{2})$	(2,1)	−580.921	$\frac{1}{2}$	$\frac{3}{2}$	2	8	$\frac{1}{2\sqrt{30}}$	$\frac{1}{15}$
$(\frac{1}{2},\frac{1}{2})$	(1,1)	−36.536	$\frac{1}{2}$	$\frac{1}{2}$	1	2	$-\frac{1}{3}$	$\frac{2}{9}$
$(\frac{3}{2},\frac{1}{2})$	(1,1)	−25.538	$\frac{1}{2}$	1	$\frac{3}{2}$	4	$-\frac{1}{6}$	$\frac{1}{9}$
$(\frac{5}{2},\frac{3}{2})$	(2,2)	−24.394	$\frac{1}{2}$	2	$\frac{5}{2}$	12	$-\frac{1}{10\sqrt{3}}$	$\frac{1}{25}$
$(\frac{3}{2},\frac{3}{2})$	(2,2)	−14.977	$\frac{1}{2}$	$\frac{3}{2}$	2	8	$-\frac{3}{10\sqrt{2}}$	$\frac{18}{50}$
$(\frac{1}{2},\frac{3}{2})$	(1,1)	+5.848	$\frac{1}{2}$	1	$\frac{3}{2}$	4	$-\frac{1}{6}$	$\frac{1}{9}$
$(\frac{5}{2},\frac{5}{2})$	(2,2)	+10.515	$\frac{1}{2}$	$\frac{5}{2}$	2	18	$\frac{\sqrt{7}}{15}$	$\frac{14}{25}$
$(\frac{3}{2},\frac{3}{2})$	(1,1)	+16.847	$\frac{1}{2}$	$\frac{3}{2}$	1	8	$\frac{\sqrt{5}}{6\sqrt{2}}$	$\frac{5}{9}$
$(\frac{3}{2},\frac{5}{2})$	(2,2)	+19.932	$\frac{1}{2}$	2	$\frac{5}{2}$	12	$-\frac{1}{10\sqrt{3}}$	$\frac{1}{25}$
$(\frac{1}{2},\frac{3}{2})$	(1,2)	+571.792	$\frac{1}{2}$	2	$\frac{3}{2}$	4	$\frac{1}{2\sqrt{3}}$	$\frac{1}{3}$
$(\frac{3}{2},\frac{3}{2})$	(1,2)	+582.790	$\frac{1}{2}$	$\frac{3}{2}$	2	8	$\frac{1}{2\sqrt{30}}$	$\frac{1}{15}$
$(\frac{3}{2},\frac{5}{2})$	(1,2)	+617.700	$\frac{1}{2}$	2	$\frac{5}{2}$	12	$-\frac{1}{2\sqrt{5}}$	$\frac{3}{5}$
$(\frac{1}{2},\frac{1}{2})$	(1,0)	+1534.050	$\frac{1}{2}$	$\frac{1}{2}$	1	2	$\frac{1}{\sqrt{6}}$	$\frac{1}{3}$
$(\frac{3}{2},\frac{1}{2})$	(1,0)	+1545.049	$\frac{1}{2}$	1	$\frac{3}{2}$	4	$-\frac{1}{\sqrt{6}}$	$\frac{2}{3}$

[a] $F = I_H + F_1$ and $F_1 = J + I_N$, where $I_N = 1$ and $I_H = \frac{1}{2}$.
[b] Frequency offset in kilohertz (kHz) relative to 23694.495487 kHz (Kukolich [1967], Table I [calculated]).

TABLE 16

$F_1 - I_H$ HYPERFINE FREQUENCIES AND INTENSITIES FOR NH$_3$ (2,2)

$F' \rightarrow F$ [a]	$F'_1 \rightarrow F_1$ [a]	$\Delta\nu_{HF}$ [b] (kHz)	a	b	c	$\frac{(2F'+1)(2F+1)}{(2I_H+1)}$	6j	$R_i(F, F_1)$
$(\frac{3}{2},\frac{3}{2})$	(1,2)	−2099.027	$\frac{1}{2}$	$\frac{3}{2}$	2	8	$\frac{1}{2\sqrt{30}}$	$\frac{1}{15}$
$(\frac{3}{2},\frac{5}{2})$	(1,2)	−2058.265	$\frac{1}{2}$	2	$\frac{5}{2}$	12	$-\frac{1}{2\sqrt{5}}$	$\frac{3}{5}$
$(\frac{1}{2},\frac{3}{2})$	(1,2)	−2053.464	$\frac{1}{2}$	2	$\frac{3}{2}$	4	$\frac{1}{2\sqrt{3}}$	$\frac{1}{3}$
$(\frac{7}{2},\frac{5}{2})$	(3,2)	−1297.079	$\frac{1}{2}$	3	$\frac{7}{2}$	24	$-\frac{1}{\sqrt{42}}$	$\frac{4}{7}$
$(\frac{5}{2},\frac{3}{2})$	(3,2)	−1296.096	$\frac{1}{2}$	3	$\frac{5}{2}$	12	$\frac{1}{\sqrt{30}}$	$\frac{6}{15}$
$(\frac{5}{2},\frac{5}{2})$	(3,2)	−1255.335	$\frac{1}{2}$	$\frac{5}{2}$	3	18	$\frac{1}{3\sqrt{70}}$	$\frac{1}{35}$
$(\frac{3}{2},\frac{1}{2})$	(1,1)	−44.511	$\frac{1}{2}$	1	$\frac{3}{2}$	4	$-\frac{1}{6}$	$\frac{1}{9}$
$(\frac{5}{2},\frac{3}{2})$	(2,2)	−41.813	$\frac{1}{2}$	2	$\frac{5}{2}$	12	$-\frac{1}{10\sqrt{3}}$	$\frac{1}{25}$
$(\frac{7}{2},\frac{5}{2})$	(3,3)	−41.444	$\frac{1}{2}$	3	$\frac{7}{2}$	24	$-\frac{1}{14\sqrt{6}}$	$\frac{1}{49}$

TABLE 16 (*Continued*)

$F' \to F$ [a]	$F_1' \to F_1$ [a]	$\Delta\nu_{HF}$ [b] (kHz)	a	b	c	$\frac{(2F'+1)(2F+1)}{(2I_H+1)}$	6j	$R_i(F,F_1)$
$(\frac{5}{2},\frac{5}{2})$	(2,2)	−1.051	$\frac{1}{2}$	$\frac{5}{2}$	2	18	$\frac{\sqrt{7}}{15}$	$\frac{14}{25}$
$(\frac{3}{2},\frac{3}{2})$	(2,2)	−1.051	$\frac{1}{2}$	$\frac{3}{2}$	2	8	$-\frac{3}{10\sqrt{2}}$	$\frac{9}{25}$
$(\frac{7}{2},\frac{7}{2})$	(3,3)	+0.309	$\frac{1}{2}$	$\frac{7}{2}$	3	32	$\frac{3\sqrt{3}}{28\sqrt{2}}$	$\frac{27}{49}$
$(\frac{5}{2},\frac{5}{2})$	(3,3)	+0.309	$\frac{1}{2}$	$\frac{5}{2}$	3	18	$-\frac{\sqrt{10}}{21}$	$\frac{20}{49}$
$(\frac{3}{2},\frac{3}{2})$	(1,1)	+1.054	$\frac{1}{2}$	$\frac{3}{2}$	1	8	$\frac{\sqrt{5}}{6\sqrt{2}}$	$\frac{5}{9}$
$(\frac{1}{2},\frac{1}{2})$	(1,1)	+1.054	$\frac{1}{2}$	$\frac{1}{2}$	1	2	$-\frac{1}{3}$	$\frac{2}{9}$
$(\frac{3}{2},\frac{5}{2})$	(2,2)	+39.710	$\frac{1}{2}$	2	$\frac{5}{2}$	12	$-\frac{1}{10\sqrt{3}}$	$\frac{1}{25}$
$(\frac{5}{2},\frac{7}{2})$	(3,3)	+42.045	$\frac{1}{2}$	3	$\frac{7}{2}$	24	$-\frac{1}{14\sqrt{6}}$	$\frac{1}{49}$
$(\frac{1}{2},\frac{3}{2})$	(1,1)	+46.614	$\frac{1}{2}$	1	$\frac{3}{2}$	4	$-\frac{1}{6}$	$\frac{1}{9}$
$(\frac{5}{2},\frac{5}{2})$	(2,3)	+1254.584	$\frac{1}{2}$	$\frac{5}{2}$	3	18	$\frac{1}{3\sqrt{70}}$	$\frac{1}{35}$
$(\frac{3}{2},\frac{5}{2})$	(2,3)	+1295.345	$\frac{1}{2}$	3	$\frac{5}{2}$	12	$\frac{1}{\sqrt{30}}$	$\frac{6}{15}$
$(\frac{5}{2},\frac{7}{2})$	(2,3)	+1296.328	$\frac{1}{2}$	3	$\frac{7}{2}$	24	$-\frac{1}{\sqrt{42}}$	$\frac{4}{7}$
$(\frac{3}{2},\frac{1}{2})$	(2,1)	+2053.464	$\frac{1}{2}$	2	$\frac{3}{2}$	4	$\frac{1}{2\sqrt{3}}$	$\frac{1}{3}$
$(\frac{5}{2},\frac{3}{2})$	(2,1)	+2058.265	$\frac{1}{2}$	2	$\frac{5}{2}$	12	$-\frac{1}{2\sqrt{5}}$	$\frac{3}{5}$
$(\frac{3}{2},\frac{3}{2})$	(2,1)	+2099.027	$\frac{1}{2}$	$\frac{3}{2}$	2	8	$\frac{1}{2\sqrt{30}}$	$\frac{1}{15}$

[a] $F = I_H + F_1$ and $F_1 = J + I_N$, where $I_N = 1$ and $I_H = \frac{1}{2}$.
[b] Frequency offset in kilohertz (kHz) relative to 23722633.335 kHz (Kukolich [1967] Table II [calculated]).

TABLE 17
F_1-I_H HYPERFINE FREQUENCIES AND INTENSITIES FOR NH$_3$ (3,3)

$F' \to F$ [a]	$F_1' \to F_1$ [a]	$\Delta\nu_{HF}$ [b] (kHz)	a	b	c	$\frac{(2F'+1)(2F+1)}{(2I_H+1)}$	6j	$R_i(F,F_1)$
$(\frac{7}{2},\frac{9}{2})$	(2,3)	−2324.577	$\frac{3}{2}$	3	$\frac{9}{2}$	20	$-\frac{1}{2\sqrt{14}}$	$\frac{5}{14}$
$(\frac{5}{2},\frac{7}{2})$	(2,3)	−2312.558	$\frac{3}{2}$	3	$\frac{7}{2}$	12	$-\frac{1}{7}$	$\frac{12}{49}$
$(\frac{1}{2},\frac{3}{2})$	(2,3)	−2304.415	$\frac{3}{2}$	3	$\frac{3}{2}$	2	$\frac{1}{2\sqrt{5}}$	$\frac{1}{10}$
$(\frac{3}{2},\frac{5}{2})$	(2,3)	−2301.989	$\frac{3}{2}$	3	$\frac{5}{2}$	6	$-\frac{\sqrt{2}}{5\sqrt{3}}$	$\frac{4}{25}$
$(\frac{7}{2},\frac{7}{2})$	(2,3)	…	$\frac{3}{2}$	$\frac{7}{2}$	3	16	$\frac{1}{14\sqrt{2}}$	$\frac{2}{49}$
$(\frac{5}{2},\frac{5}{2})$	(2,3)	…	$\frac{3}{2}$	$\frac{5}{2}$	3	9	$-\frac{8}{105}$	$\frac{64}{1225}$
$(\frac{3}{2},\frac{3}{2})$	(2,3)	…	$\frac{3}{2}$	$\frac{3}{2}$	3	4	$\frac{1}{10}$	$\frac{1}{25}$
$(\frac{7}{2},\frac{5}{2})$	(2,3)	…	$\frac{3}{2}$	$\frac{5}{2}$	3	12	$-\frac{1}{14\sqrt{30}}$	$\frac{1}{490}$
$(\frac{5}{2},\frac{3}{2})$	(2,3)	…	$\frac{3}{2}$	$\frac{3}{2}$	3	6	$\frac{1}{10\sqrt{21}}$	$\frac{1}{350}$
$(\frac{7}{2},\frac{5}{2})$	(4,3)	−1690.763	$\frac{3}{2}$	4	$\frac{7}{2}$	12	$-\frac{5}{28\sqrt{2}}$	$\frac{150}{784}$
$(\frac{9}{2},\frac{7}{2})$	(4,3)	−1689.154	$\frac{3}{2}$	4	$\frac{9}{2}$	20	$\frac{\sqrt{11}}{12\sqrt{6}}$	$\frac{110}{432}$
$(\frac{5}{2},\frac{3}{2})$	(4,3)	−1682.925	$\frac{3}{2}$	4	$\frac{5}{2}$	6	$\frac{1}{\sqrt{42}}$	$\frac{1}{7}$
$(\frac{11}{2},\frac{9}{2})$	(4,3)	−1679.029	$\frac{3}{2}$	4	$\frac{11}{2}$	30	$-\frac{1}{3\sqrt{10}}$	$\frac{1}{3}$
$(\frac{9}{2},\frac{9}{2})$	(4,3)	…	$\frac{3}{2}$	$\frac{9}{2}$	4	25	$\frac{1}{6\sqrt{30}}$	$\frac{5}{216}$
$(\frac{7}{2},\frac{7}{2})$	(4,3)	…	$\frac{3}{2}$	$\frac{7}{2}$	4	16	$-\frac{\sqrt{5}}{21\sqrt{6}}$	$\frac{40}{1323}$
$(\frac{5}{2},\frac{5}{2})$	(4,3)	…	$\frac{3}{2}$	$\frac{5}{2}$	4	9	$\frac{1}{14\sqrt{2}}$	$\frac{9}{392}$
$(\frac{5}{2},\frac{7}{2})$	(4,3)	…	$\frac{3}{2}$	3	$\frac{7}{2}$	12	$\frac{1}{84\sqrt{2}}$	$\frac{1}{1176}$
$(\frac{7}{2},\frac{9}{2})$	(4,3)	…	$\frac{3}{2}$	3	$\frac{9}{2}$	20	$-\frac{1}{12\sqrt{210}}$	$\frac{1}{1512}$
$(\frac{7}{2},\frac{5}{2})$	(2,2)	…	$\frac{3}{2}$	2	$\frac{7}{2}$	12	$-\frac{1}{\sqrt{210}}$	$\frac{6}{105}$
$(\frac{5}{2},\frac{3}{2})$	(2,2)	−80.030	$\frac{3}{2}$	2	$\frac{5}{2}$	6	$\frac{\sqrt{7}}{10\sqrt{6}}$	$\frac{7}{100}$
$(\frac{3}{2},\frac{1}{2})$	(2,2)	…	$\frac{3}{2}$	2	$\frac{3}{2}$	2	$-\frac{1}{2\sqrt{10}}$	$\frac{1}{20}$
$(\frac{5}{2},\frac{3}{2})$	(3,3)	−64.182	$\frac{3}{2}$	3	$\frac{5}{2}$	6	$-\frac{1}{\sqrt{210}}$	$\frac{3}{105}$
$(\frac{7}{2},\frac{5}{2})$	(3,3)	…	$\frac{3}{2}$	3	$\frac{7}{2}$	12	$\frac{\sqrt{5}}{28\sqrt{2}}$	$\frac{15}{392}$
$(\frac{9}{2},\frac{7}{2})$	(3,3)	−61.951	$\frac{3}{2}$	3	$\frac{9}{2}$	20	$-\frac{1}{4\sqrt{42}}$	$\frac{5}{168}$
$(\frac{11}{2},\frac{9}{2})$	(4,4)	−50.048	$\frac{3}{2}$	4	$\frac{11}{2}$	30	$-\frac{1}{5\sqrt{66}}$	$\frac{1}{55}$

TABLE 17 (*Continued*)

$F' \to F$[a]	$F_1' \to F_1$[a]	$\Delta\nu_{HF}$[b] (kHz)	a	b	c	$\frac{(2F'+1)(2F+1)}{(2I_H+1)}$	6j	$R_i(F, F_1)$
$(\frac{9}{2},\frac{7}{2})$	(4,4)	...	$\frac{3}{2}$	4	$\frac{9}{2}$	20	$\frac{\sqrt{77}}{180\sqrt{2}}$	$\frac{77}{3240}$
$(\frac{7}{2},\frac{5}{2})$	(4,4)	...	$\frac{3}{2}$	4	$\frac{7}{2}$	12	$-\frac{1}{4\sqrt{42}}$	$\frac{1}{56}$
$(\frac{3}{2},\frac{3}{2})$	(3,3)	−1.334	$\frac{3}{2}$	$\frac{3}{2}$	3	4	$-\frac{1}{\sqrt{35}}$	$\frac{4}{35}$
$(\frac{9}{2},\frac{9}{2})$	(3,3)	...	$\frac{3}{2}$	$\frac{9}{2}$	3	25	$\frac{\sqrt{11}}{2\sqrt{210}}$	$\frac{275}{840}$
$(\frac{7}{2},\frac{7}{2})$	(3,3)	...	$\frac{3}{2}$	$\frac{7}{2}$	3	16	$-\frac{\sqrt{2}}{7\sqrt{3}}$	$\frac{32}{147}$
$(\frac{5}{2},\frac{5}{2})$	(3,3)	...	$\frac{3}{2}$	$\frac{5}{2}$	3	9	$\frac{17}{42\sqrt{10}}$	$\frac{2601}{17640}$
$(\frac{5}{2},\frac{5}{2})$	(4,4)	+0.445	$\frac{3}{2}$	$\frac{5}{2}$	4	9	$-\frac{5}{6\sqrt{42}}$	$\frac{25}{168}$
$(\frac{7}{2},\frac{7}{2})$	(4,4)	...	$\frac{3}{2}$	$\frac{7}{2}$	4	16	$\frac{4\sqrt{2}}{9\sqrt{35}}$	$\frac{512}{2835}$
$(\frac{9}{2},\frac{9}{2})$	(4,4)	...	$\frac{3}{2}$	$\frac{9}{2}$	4	25	$-\frac{41}{90\sqrt{22}}$	$\frac{1681}{7128}$
$(\frac{11}{2},\frac{11}{2})$	(4,4)	...	$\frac{3}{2}$	$\frac{11}{2}$	4	36	$\frac{\sqrt{13}}{3\sqrt{165}}$	$\frac{52}{165}$
$(\frac{1}{2},\frac{1}{2})$	(2,2)	+1.067	$\frac{3}{2}$	$\frac{1}{2}$	2	1	$-\frac{1}{2\sqrt{5}}$	$\frac{1}{20}$
$(\frac{3}{2},\frac{3}{2})$	(2,2)	...	$\frac{3}{2}$	$\frac{3}{2}$	2	4	$\frac{1}{5\sqrt{2}}$	$\frac{2}{25}$
$(\frac{5}{2},\frac{5}{2})$	(2,2)	...	$\frac{3}{2}$	$\frac{5}{2}$	2	9	$-\frac{11}{3\sqrt{7}}$	$\frac{1089}{6300}$
$(\frac{7}{2},\frac{7}{2})$	(2,2)	...	$\frac{3}{2}$	$\frac{7}{2}$	2	16	$\frac{\sqrt{3}}{2\sqrt{35}}$	$\frac{12}{35}$
$(\frac{9}{2},\frac{11}{2})$	(4,4)	+50.937	$\frac{3}{2}$	4	$\frac{11}{2}$	30	$-\frac{1}{5\sqrt{66}}$	$\frac{1}{55}$
$(\frac{7}{2},\frac{9}{2})$	(4,4)	...	$\frac{3}{2}$	4	$\frac{9}{2}$	20	$\frac{\sqrt{77}}{180\sqrt{2}}$	$\frac{77}{3240}$
$(\frac{5}{2},\frac{7}{2})$	(4,4)	...	$\frac{3}{2}$	4	$\frac{7}{2}$	12	$-\frac{1}{4\sqrt{42}}$	$\frac{1}{56}$
$(\frac{7}{2},\frac{9}{2})$	(3,3)	+59.283	$\frac{3}{2}$	3	$\frac{9}{2}$	20	$-\frac{1}{4\sqrt{42}}$	$\frac{5}{168}$
$(\frac{5}{2},\frac{7}{2})$	(3,3)	...	$\frac{3}{2}$	3	$\frac{7}{2}$	12	$\frac{\sqrt{5}}{28\sqrt{2}}$	$\frac{15}{392}$
$(\frac{3}{2},\frac{5}{2})$	(3,3)	...	$\frac{3}{2}$	3	$\frac{5}{2}$	6	$-\frac{1}{\sqrt{210}}$	$\frac{3}{105}$
$(\frac{1}{2},\frac{3}{2})$	(2,2)	...	$\frac{3}{2}$	2	$\frac{3}{2}$	2	$-\frac{1}{2\sqrt{10}}$	$\frac{1}{20}$
$(\frac{3}{2},\frac{5}{2})$	(2,2)	+82.164	$\frac{3}{2}$	2	$\frac{5}{2}$	6	$\frac{\sqrt{7}}{10\sqrt{6}}$	$\frac{7}{100}$
$(\frac{5}{2},\frac{7}{2})$	(2,2)	...	$\frac{3}{2}$	2	$\frac{7}{2}$	12	$-\frac{1}{\sqrt{210}}$	$\frac{6}{105}$
$(\frac{3}{2},\frac{5}{2})$	(3,4)	+1682.036	$\frac{3}{2}$	4	$\frac{5}{2}$	6	$\frac{1}{\sqrt{42}}$	$\frac{1}{7}$
$(\frac{7}{2},\frac{9}{2})$	(3,4)	+1688.264	$\frac{3}{2}$	4	$\frac{9}{2}$	20	$\frac{\sqrt{11}}{12\sqrt{6}}$	$\frac{55}{216}$
$(\frac{5}{2},\frac{7}{2})$	(3,4)	+1689.873	$\frac{3}{2}$	4	$\frac{7}{2}$	12	$-\frac{5}{28\sqrt{2}}$	$\frac{75}{392}$
$(\frac{9}{2},\frac{11}{2})$	(3,4)	+1678.140	$\frac{3}{2}$	4	$\frac{11}{2}$	30	$-\frac{1}{3\sqrt{10}}$	$\frac{1}{3}$
$(\frac{9}{2},\frac{7}{2})$	(3,4)	...	$\frac{3}{2}$	$\frac{7}{2}$	4	20	$-\frac{1}{12\sqrt{210}}$	$\frac{1}{1512}$
$(\frac{7}{2},\frac{5}{2})$	(3,4)	...	$\frac{3}{2}$	$\frac{5}{2}$	4	12	$\frac{1}{84\sqrt{2}}$	$\frac{1}{1176}$
$(\frac{9}{2},\frac{9}{2})$	(3,4)	...	$\frac{3}{2}$	$\frac{9}{2}$	4	25	$\frac{1}{6\sqrt{30}}$	$\frac{5}{216}$
$(\frac{7}{2},\frac{7}{2})$	(3,4)	...	$\frac{3}{2}$	$\frac{7}{2}$	4	16	$-\frac{\sqrt{5}}{21\sqrt{6}}$	$\frac{40}{1323}$
$(\frac{5}{2},\frac{5}{2})$	(3,4)	...	$\frac{3}{2}$	$\frac{5}{2}$	4	9	$\frac{1}{14\sqrt{2}}$	$\frac{9}{392}$
$(\frac{5}{2},\frac{3}{2})$	(3,2)	+2301.723	$\frac{3}{2}$	3	$\frac{5}{2}$	6	$-\frac{\sqrt{2}}{5\sqrt{3}}$	$\frac{4}{25}$
$(\frac{3}{2},\frac{1}{2})$	(3,2)	+2304.148	$\frac{3}{2}$	3	$\frac{3}{2}$	2	$\frac{1}{2\sqrt{5}}$	$\frac{1}{10}$
$(\frac{7}{2},\frac{5}{2})$	(3,2)	+2312.291	$\frac{3}{2}$	3	$\frac{7}{2}$	12	$\frac{1}{7}$	$\frac{12}{49}$
$(\frac{9}{2},\frac{7}{2})$	(3,2)	+2324.310	$\frac{3}{2}$	3	$\frac{9}{2}$	20	$-\frac{1}{2\sqrt{14}}$	$\frac{5}{14}$
$(\frac{5}{2},\frac{7}{2})$	(3,2)	...	$\frac{3}{2}$	2	$\frac{7}{2}$	12	$-\frac{1}{14\sqrt{30}}$	$\frac{1}{490}$
$(\frac{3}{2},\frac{5}{2})$	(3,2)	...	$\frac{3}{2}$	2	$\frac{5}{2}$	6	$\frac{1}{10\sqrt{21}}$	$\frac{1}{350}$
$(\frac{3}{2},\frac{3}{2})$	(3,2)	...	$\frac{3}{2}$	$\frac{3}{2}$	3	4	$\frac{1}{10}$	$\frac{1}{25}$
$(\frac{5}{2},\frac{5}{2})$	(3,2)	...	$\frac{3}{2}$	$\frac{5}{2}$	3	9	$-\frac{8}{105}$	$\frac{64}{1225}$
$(\frac{7}{2},\frac{7}{2})$	(3,2)	...	$\frac{3}{2}$	$\frac{7}{2}$	3	16	$\frac{1}{14\sqrt{2}}$	$\frac{2}{49}$

[a] $F = I_H + F_1$ and $F_1 = J + I_N$, where $I_N = 1$ and $I_H = \frac{3}{2}$.
[b] Frequency offset in kilohertz (kHz) relative to 23870129.183 kHz (Kukolich [1967] Table III [calculated]).

TABLE 18
F_1–I_H Hyperfine Frequencies and Intensities for NH_3 (4,4)

$F' \to F$[a]	$F'_1 \to F_1$[a]	$\Delta\nu_{HF}$[b] (kHz)	a	b	c	$\frac{(2F'+1)(2F+1)}{(2I_H+1)}$	6j	$R_i(F,F_1)$
$(\frac{7}{2},\frac{9}{2})$	(3,4)	−2485.883	$\frac{1}{2}$	4	$\frac{9}{2}$	40	$-\frac{1}{6\sqrt{2}}$	$\frac{5}{9}$
$(\frac{5}{2},\frac{7}{2})$	(3,4)	−2481.291	$\frac{1}{2}$	4	$\frac{7}{2}$	24	$\frac{1}{2\sqrt{14}}$	$\frac{3}{7}$
$(\frac{7}{2},\frac{7}{2})$	(3,4)	...	$\frac{1}{2}$	$\frac{7}{2}$	4	32	$\frac{1}{12\sqrt{14}}$	$\frac{1}{63}$
$(\frac{9}{2},\frac{7}{2})$	(5,4)	−1924.144	$\frac{1}{2}$	5	$\frac{9}{2}$	40	$\frac{1}{3\sqrt{10}}$	$\frac{4}{9}$
$(\frac{11}{2},\frac{9}{2})$	(5,4)	−1922.222	$\frac{1}{2}$	5	$\frac{11}{2}$	60	$-\frac{1}{\sqrt{110}}$	$\frac{6}{11}$
$(\frac{9}{2},\frac{9}{2})$	(5,4)	...	$\frac{1}{2}$	$\frac{9}{2}$	5	50	$\frac{1}{15\sqrt{22}}$	$\frac{1}{99}$
$(\frac{9}{2},\frac{9}{2})$	(4,4)	...	$\frac{1}{2}$	$\frac{9}{2}$	4	50	$\frac{\sqrt{22}}{45}$	$\frac{44}{81}$
$(\frac{7}{2},\frac{7}{2})$	(4,4)	−1.448	$\frac{1}{2}$	$\frac{7}{2}$	4	32	$-\frac{\sqrt{35}}{36\sqrt{2}}$	$\frac{35}{81}$
$(\frac{9}{2},\frac{7}{2})$	(4,4)	...	$\frac{1}{2}$	4	$\frac{9}{2}$	40	$-\frac{1}{18\sqrt{10}}$	$\frac{1}{81}$
$(\frac{7}{2},\frac{9}{2})$	(4,4)	...	$\frac{1}{2}$	4	$\frac{9}{2}$	40	$-\frac{1}{18\sqrt{10}}$	$\frac{1}{81}$
$(\frac{11}{2},\frac{11}{2})$	(5,5)	...	$\frac{1}{2}$	$\frac{11}{2}$	5	72	$\frac{\sqrt{65}}{66\sqrt{2}}$	$\frac{65}{121}$
$(\frac{9}{2},\frac{9}{2})$	(5,5)	+0.526	$\frac{1}{2}$	$\frac{9}{2}$	5	50	$-\frac{3\sqrt{3}}{55}$	$\frac{54}{121}$
$(\frac{11}{2},\frac{9}{2})$	(5,5)	...	$\frac{1}{2}$	5	$\frac{11}{2}$	60	$-\frac{1}{22\sqrt{15}}$	$\frac{1}{121}$
$(\frac{9}{2},\frac{11}{2})$	(5,5)	...	$\frac{1}{2}$	5	$\frac{11}{2}$	60	$-\frac{1}{22\sqrt{15}}$	$\frac{1}{121}$
$(\frac{7}{2},\frac{7}{2})$	(3,3)	...	$\frac{1}{2}$	$\frac{7}{2}$	3	32	$\frac{3\sqrt{3}}{28\sqrt{2}}$	$\frac{27}{49}$
$(\frac{5}{2},\frac{5}{2})$	(3,3)	...	$\frac{1}{2}$	$\frac{5}{2}$	3	18	$-\frac{\sqrt{10}}{21}$	$\frac{20}{49}$
$(\frac{7}{2},\frac{5}{2})$	(3,3)	...	$\frac{1}{2}$	3	$\frac{7}{2}$	24	$-\frac{1}{14\sqrt{6}}$	$\frac{1}{49}$
$(\frac{5}{2},\frac{7}{2})$	(3,3)	...	$\frac{1}{2}$	3	$\frac{7}{2}$	24	$-\frac{1}{14\sqrt{6}}$	$\frac{1}{49}$
$(\frac{9}{2},\frac{11}{2})$	(4,5)	+1931.301	$\frac{1}{2}$	5	$\frac{11}{2}$	60	$-\frac{1}{\sqrt{110}}$	$\frac{6}{11}$
$(\frac{7}{2},\frac{9}{2})$	(4,5)	+1923.222	$\frac{1}{2}$	5	$\frac{9}{2}$	40	$\frac{1}{3\sqrt{10}}$	$\frac{4}{9}$
$(\frac{9}{2},\frac{9}{2})$	(4,5)	...	$\frac{1}{2}$	$\frac{9}{2}$	5	50	$\frac{1}{15\sqrt{22}}$	$\frac{1}{99}$
$(\frac{7}{2},\frac{5}{2})$	(4,3)	+2480.878	$\frac{1}{2}$	4	$\frac{7}{2}$	24	$\frac{1}{2\sqrt{14}}$	$\frac{3}{7}$
$(\frac{9}{2},\frac{7}{2})$	(4,3)	+2485.470	$\frac{1}{2}$	4	$\frac{9}{2}$	40	$-\frac{1}{6\sqrt{2}}$	$\frac{5}{9}$
$(\frac{7}{2},\frac{7}{2})$	(4,3)	...	$\frac{1}{2}$	$\frac{7}{2}$	4	32	$\frac{1}{12\sqrt{14}}$	$\frac{1}{63}$

[a] $F = I_H + F_1$ and $F_1 = J + I_N$, where $I_N = 1$ and $I_H = \frac{1}{2}$.
[b] Frequency offset in kilohertz (kHz) relative to 24139416.34 kHz (Kukolich & Wofsy [1970], Table II [calculated])

TABLE 19
Hyperfine Intensities for NH_3 (1,1)

$F' \to F$	$F'_1 \to F_1$	$J' \to J$	$R_i(F_1,J)R_i(F,F_1)$[a,b]
$(\frac{1}{2},\frac{1}{2})$	(0,1)	(1,1)	$\frac{1}{27}$
$(\frac{1}{2},\frac{3}{2})$	(0,1)	(1,1)	$\frac{2}{27}$
$(\frac{3}{2},\frac{1}{2})$	(2,1)	(1,1)	$\frac{5}{108}$
$(\frac{5}{2},\frac{3}{2})$	(2,1)	(1,1)	$\frac{1}{12}$
$(\frac{3}{2},\frac{3}{2})$	(2,1)	(1,1)	$\frac{1}{108}$
$(\frac{1}{2},\frac{1}{2})$	(1,1)	(1,1)	$\frac{2}{108}$
$(\frac{3}{2},\frac{1}{2})$	(1,1)	(1,1)	$\frac{1}{108}$
$(\frac{5}{2},\frac{3}{2})$	(2,2)	(1,1)	$\frac{1}{60}$
$(\frac{3}{2},\frac{3}{2})$	(2,2)	(1,1)	$\frac{3}{20}$
$(\frac{1}{2},\frac{3}{2})$	(1,1)	(1,1)	$\frac{1}{108}$
$(\frac{5}{2},\frac{5}{2})$	(2,2)	(1,1)	$\frac{7}{30}$
$(\frac{3}{2},\frac{3}{2})$	(1,1)	(1,1)	$\frac{5}{108}$
$(\frac{3}{2},\frac{5}{2})$	(2,2)	(1,1)	$\frac{1}{60}$
$(\frac{1}{2},\frac{3}{2})$	(1,2)	(1,1)	$\frac{5}{108}$
$(\frac{3}{2},\frac{3}{2})$	(1,2)	(1,1)	$\frac{1}{108}$
$(\frac{3}{2},\frac{5}{2})$	(1,2)	(1,1)	$\frac{1}{12}$
$(\frac{1}{2},\frac{1}{2})$	(1,0)	(1,1)	$\frac{1}{27}$

TABLE 19 (*Continued*)

$F' \to F$	$F'_1 \to F_1$	$J' \to J$	$R_i(F_1,J)R_i(F,F_1)$[a,b]
$(\frac{3}{2},\frac{1}{2})$	(1,0)	(1,1)	$\frac{2}{27}$

[a] Compare with Kukolich (1967), Table IX, after scaling R_i by $(2I_H+1)(2I_N+1) = 6$ (Kukolich [1967] lists unnormalized line strengths in their Table IX).
[b] Note that the sum of the relative intensities $\sum_i R_i = 1.0$.

TABLE 20
Hyperfine Intensities for NH_3 (2,2)

$F' \to F$	$F'_1 \to F_1$	$J' \to J$	$R_i(F_1,J)\,R_i(F,F_1)$[a,b]
$(\frac{3}{2},\frac{3}{2})$	(1,2)	(2,2)	$\frac{1}{300}$
$(\frac{3}{2},\frac{5}{2})$	(1,2)	(2,2)	$\frac{3}{100}$
$(\frac{1}{2},\frac{3}{2})$	(1,2)	(2,2)	$\frac{1}{60}$
$(\frac{7}{2},\frac{5}{2})$	(3,2)	(2,2)	$\frac{4}{135}$
$(\frac{5}{2},\frac{3}{2})$	(3,2)	(2,2)	$\frac{14}{675}$
$(\frac{5}{2},\frac{5}{2})$	(3,2)	(2,2)	$\frac{1}{675}$
$(\frac{3}{2},\frac{1}{2})$	(1,1)	(2,2)	$\frac{1}{60}$

TABLE 20 (*Continued*)

$F' \to F$	$F_1' \to F_1$	$J' \to J$	$R_i(F_1, J)\ R_i(F, F_1)$[a,b]
$(\frac{5}{2}, \frac{3}{2})$	(2,2)	(2,2)	$\frac{1}{108}$
$(\frac{7}{2}, \frac{5}{2})$	(3,3)	(2,2)	$\frac{8}{945}$
$(\frac{5}{2}, \frac{5}{2})$	(2,2)	(2,2)	$\frac{7}{54}$
$(\frac{3}{2}, \frac{3}{2})$	(2,2)	(2,2)	$\frac{1}{12}$
$(\frac{7}{2}, \frac{7}{2})$	(3,3)	(2,2)	$\frac{8}{35}$
$(\frac{5}{2}, \frac{5}{2})$	(3,3)	(2,2)	$\frac{32}{189}$
$(\frac{3}{2}, \frac{3}{2})$	(1,1)	(2,2)	$\frac{1}{12}$
$(\frac{1}{2}, \frac{1}{2})$	(1,1)	(2,2)	$\frac{1}{30}$
$(\frac{3}{2}, \frac{5}{2})$	(2,2)	(2,2)	$\frac{1}{108}$
$(\frac{5}{2}, \frac{7}{2})$	(3,3)	(2,2)	$\frac{8}{945}$
$(\frac{1}{2}, \frac{3}{2})$	(1,1)	(2,2)	$\frac{1}{60}$

TABLE 20 (*Continued*)

$F' \to F$	$F_1' \to F_1$	$J' \to J$	$R_i(F_1, J)\ R_i(F, F_1)$[a,b]
$(\frac{5}{2}, \frac{5}{2})$	(2,3)	(2,2)	$\frac{1}{675}$
$(\frac{3}{2}, \frac{5}{2})$	(2,3)	(2,2)	$\frac{14}{675}$
$(\frac{5}{2}, \frac{7}{2})$	(2,3)	(2,2)	$\frac{4}{135}$
$(\frac{3}{2}, \frac{1}{2})$	(2,1)	(2,2)	$\frac{1}{60}$
$(\frac{5}{2}, \frac{3}{2})$	(2,1)	(2,2)	$\frac{3}{100}$
$(\frac{3}{2}, \frac{3}{2})$	(2,1)	(2,2)	$\frac{1}{300}$

[a] Compare with Kukolich (1967), Table IX, after scaling R_i by $(2I_H + 1)(2I_N + 1) = 6$ (Kukolich [1967] lists unnormalized line strengths in their Table IX).

[b] Note that the sum of the relative intensities $\sum_i R_i = 1.0$.

REFERENCES

Bachiller, R., et al. 1997, A&A, 319, 235

Brinch, C., & Hogerheijde, M. R. 2010, A&A, 523, A 25

Caselli, P., Myers, P. C., & Thaddeus, P. 1995, ApJ, 455, L 77

Cross, P. C., Hainer, R. M., & King, G. C. 1944, J. Chem. Phys., 12, 210

Daniel, F., Cernicharo, J., & Dubernet, M.-L. 2006, ApJ, 648, 461

Draine, B. T. 2011, Physics of the Interstellar and Intergalactic Medium (Princeton: Princeton Univ. Press)

Edmonds, A. R. 1960, Angular Momentum in Quantum Mechanics (Princeton: Princeton Univ. Press)

Evans, N. J., II. 1999, ARA&A, 37, 311

Evans, N. J., II, Lacy, J. H., & Carr, J. S. 1991, ApJ, 383, 674

Evans, N. J., II, Morris, G., Sato, T., & Zuckerman, B. 1975, ApJ, 196, 433

Garrison, B. J., Lester, Jr., W. A. Miller, W. H., & Green, S. 1975, ApJ, 200, L 175

Genzel, R. 1991, in NATO Advanced Science Institutes (ASI) Ser. C, Vol. 342, ed. C. J. Lada, & N. D. Kylafis, 155

Goldsmith, P. F., & Langer, W. D. 1999, ApJ, 517, 209

Gordy, W., & Cook, R. L. 1984, Microwave Molecular Spectra (New York: Interscience Pub.)

Guilloteau, S., & Baudry, A. 1981, A&A, 97, 213

Herzberg, G. 1945, Molecular Spectra and Molecular Structure, Vol. 2: Infrared and Raman Spectra of Polyatomic Molecules (Van Nostrand Reinhold Company)

Hily-Blant, P., Walmsley, M., Pineau Des Forêts, G., & Flower, D. 2010, A&A, 513, A 41

Ho, P. T. P., & Townes, C. H. 1983, ARA&A, 21, 239

Jennings, D. A., et al. 1987, J. Mol. Spectrosc., 122, 477

Klapper, G., et al. 2003, ApJ, 582, 262

Kukolich, S. G. 1967, Phys. Rev., 156, 83

Kukolich, S. G., & Wofsy, S. C. 1970, J. Chem. Phys., 52, 5477

Kwan, J., & Scoville, N. Z. 1974, NASA STI/Recon Tech. Rep. N (Washington: NASA), 75, 20199

Leung, C.-M., & Liszt, H. S. 1976, ApJ, 208, 732

Loughnane, R. M., et al. 2012, MNRAS, 420, 1367

Mangum, J. G., Darling, J., Menten, K. M., & Henkel, C. 2008, ApJ, 673, 832

Mangum, J. G., & Wootten, A. 1993, ApJS, 89, 123

Mangum, J. G., Wootten, A., & Mundy, L. G. 1992, ApJ, 388, 467

McDowell, R. S. 1988, J. Chem. Phys., 88, 356

———. 1990, J. Chem. Phys., 93, 2801

Pagani, L., Daniel, F., & Dubernet, M.-L. 2009, A&A, 494, 719

Pickett, H. M., et al. 1998, J. Quant. Spec. Radiat. Transf., 60, 883

Poynter, R. L., & Kakar, R. K. 1975, ApJS, 29, 87

Ray, R. S. 1932, Z. Phys., 78, 74

Rosolowsky, E. W., et al. 2008, ApJS, 175, 509

Schöier, F. L., van der Tak, F. F. S., van Dishoeck, E. F., & Black, J. H. 2005, A&A, 432, 369

Shirley, Y. L., Nordhaus, M. K., Grcevich, J. M., et al. 2005, ApJ, 632, 982

Shirley, Y. L., et al. 2013, ApJS, 209, 2

Sobolev, V. V. 1960, Moving Envelopes of Stars (Cambridge: Harvard Univ. Press)

Spitzer, L. 1978, Physical Processes in the Interstellar Medium (New York: Wiley)

Stutzki, J., Olberg, M., Winnewisser, G., Jackson, J. M., & Barrett, A. H. 1984, A&A, 139, 258

Stutzki, J., & Winnewisser, G. 1985, A&A, 144, 13

Tatum, J. B. 1986, ApJS, 60, 433

Townes, C. H., & Schawlow, A. L. 1975, Microwave Spectroscopy (Mineola: Dover)

Turner, B. E. 1991, ApJS, 76, 617

Ulich, B. L., & Haas, R. W. 1976, ApJS, 30, 247

van der Tak, F. F. S., Black, J. H., Schöier, F. L., Jansen, D. J., & van Dishoeck, E. F. 2007, A&A, 468, 627

Walmsley, C. M., Churchwell, E., Nash, A., & Fitzpatrick, E. 1982, ApJ, 258, L 75